

Multi-Emission Kernels for Parton Branching Algorithms

Maximilian Löschner^{1, a, d}, Simon Plätzer^{b, c, d} and Emma Simpson Dore^a

^a*Institute for Theoretical Physics, Karlsruhe Institute of Technology, Wolfgang-Gaede-Strasse 1, 76131 Karlsruhe, Germany*

^b*Institute of Physics, NAWI Graz, University of Graz, Universitätsplatz 5, A-8010 Graz, Austria*

^c*Particle Physics, Faculty of Physics, University of Vienna, Boltzmannngasse 5, A-1090 Wien, Austria*

^d*Erwin Schrödinger Institute for Mathematics and Physics, University of Vienna, Boltzmannngasse 9, A-1090 Wien*

E-mail: maximilian.loeschner@kit.edu, simon.plaetzer@uni-graz.at,
e.simpsondore@gmail.com

ABSTRACT: We introduce a general framework to construct multi-emission kernels for parton branching algorithms at the amplitude level and across different soft and collinear limits. We highlight the connection of kinematic parameterizations and recoil schemes to the underlying power counting, and discuss in detail how soft radiation can be partitioned in between different collinear configurations beyond the single-emission picture underpinning the traditional dipole and angular ordering approaches. Our work is a vital cornerstone to build parton branching algorithms which include multiply-unresolved emissions in a fully differential way, and our construction can also be used to obtain splitting functions for probabilistic algorithms or other cross-section level objects such as subtraction terms.

¹M.L. would like to dedicate this work to his father.

Contents

1	Introduction	2
2	Construction of splitting kernels	4
2.1	Decomposition of amplitudes in a physical gauge	10
2.2	Decomposing around singular limits	13
2.3	Iterating the recoil transformation	15
2.4	Local backward direction	16
2.5	Scaling of individual internal lines and vertices	16
3	Partitioning	18
3.1	Basic purpose	19
3.2	Partial fractioning partitioning algorithm	20
3.3	Subtraction (angular ordered) partitioning algorithm	23
4	Momentum mapping	25
5	Splitting kernels	28
5.1	Power counting algorithm	30
5.2	Factorisation to hard amplitude	31
5.3	Single emission case	33
5.3.1	Quark-gluon splitting	36
5.3.2	Gluon-gluon splitting	38
5.4	Two emission case	40
6	Applications and Outlook	46
7	Summary and Conclusions	48
A	Phase space factorization	51
A.1	Emission phase space	51
A.2	Emitter and recoiler phase space	52
B	Two emissions	54
B.1	Quark-gluon-gluon splitting function	54
B.2	Relation to soft and soft-collinear functions	56
C	Two emission topologies	60
D	Removal of non-leading singular contributions	65

1 Introduction

A detailed description of QCD dynamics at current and future collider experiments is vital to discriminate Standard Model background from signals of New Physics using the most advanced methods ranging from traditional event shape variables to jet substructure methods to machine learning techniques. The comparison to detailed theory predictions is vital and a large range of analytic predictions up to the most versatile Monte Carlo event generators are used in comparison to experimental data. Specifically, Monte Carlo event generators have recently seen a tremendous development regarding the simulation of the hard scattering process, and the attention has shifted to the core, parton shower, component among other developments on non-perturbative modelling. The question of how the accuracy of parton branching algorithms can be quantified, and how they can eventually be extended beyond their current approximations – both regarding resummed perturbation theory in Quantum Chromodynamics (QCD), as well as beyond the customary limit of a large number of colour charges N – has received significant attention which we will briefly review in this introduction to motivate the present work.

Parton branching algorithms have long been used in the context of analytic resummation [1], including up to next-to-leading logarithmic (NLL) accuracy for a large class of event shape variables [2] and properties of hard objects created in hadron-hadron collisions [3]. These techniques notably exploit the coherence properties of QCD and the structure of the observable such that angular ordering can be used upon azimuthal averaging to simplify the resummation procedure. They have also been the key ingredient behind designing the Herwig angular-ordered parton shower algorithm [4–7], which is thus capable of describing global event shape variables at NLL accuracy. Due to ambiguities in how recoil of the emissions is distributed at the end of the evolution, however, failures of this naive expectation may be introduced and need careful investigation [8]. Even in the case of NLL accurate coherent branching evolution, a number of shortcomings are present in these algorithms, and have motivated additional work, notably spin and colour correlations [9] as well as mass effects [10].

The biggest shortcoming, however, is the inability of coherent branching algorithms to describe observables which are sensitive to a change in colour structure from subsequent emissions beyond the dynamics accounted for by QCD coherence, and this applies already in the large- N limit. Crucially, it is the lack of a dipole-type picture which disallows coherent branching from describing these correlations, and hence there is no chance for such an evolution to account for any of the logarithmic enhancements in non-global observables. It is clear though, that non-global observables [11–13] should be setting the level of complexity which needs to be addressed for the plethora of sophisticated analysis methods employed at the currently operating hadron colliders, and projected to be used even at future e^+e^- colliders. Note however that coherent branching is in fact able to describe the exact- N structure of global event shapes at least at leading logarithmic (LL) level.

Dipole shower algorithms [14–17], on the other hand, do offer the possibility to properly resum non-global effects at leading colour (and in fact have been used, in a specialized form, for specifically this task [11, 12]). Despite the fact that they have been used to try and

extend parton branching beyond the leading order [18], their initial accuracy remained unclear and has been proven to be wrong at various levels for global observables [19–21]. Recent work has therefore focused on trying to combine the best of dipole and coherent branching algorithms such as to maintain the accuracy for global event shapes, and a proper (*i.e.* at least leading-colour and leading logarithmic accurate) description of non-global observables [22, 23]. Within this context it turned out that recoils can cause severe accuracy problems, and that there is a delicate interplay between ordering, recoil and the question of how the soft behaviour is distributed across the partonic systems competing to emit the next parton, a mechanism typically referred to as ‘partitioning’. Notice that a dipole-type picture, or extensions thereof, is also required to have accurate control over recoils distributed emission by emission, something which is extremely important when trying to combine with fixed-order QCD calculations, either through matching or merging. Most of the time, the development of parton showers within this context has been closely tied to the development of fixed-order subtraction terms reflecting the singularity structure of QCD *cross sections* for the emission of one, or possibly two, unresolved partons.

The shortcomings of existing parton shower algorithms, and possible improvements, have been addressed in [19] by checking how well they reproduce the soft radiation pattern for two subsequent emissions, while [21] has been taking a different point of view in starting from formulating parton branching algorithms at the amplitude level [24]. This is a theoretical framework which addresses the iterative build-up of an amplitude (and its conjugate) describing the emission of multiple unresolved partons, and is thus the prime framework to analyse how cross sections can be described in the limit of a large number of unresolved partons. A systematic expansion of the resulting expressions around the large- N limit, for example, then leads to commonly used parton branching algorithms which can be extended beyond the large- N limit. The same formalism can also be used to derive further limiting cases such as coherent branching, which has ultimately led to the proposal of an improved dipole shower algorithm. We stress that only within such a framework, and similar approaches pursued by Nagy and Soper [25], is it possible to analyse the entire set of correlations in between multiple emissions, and to systematically obtain an approximation of the iterations, rather than iterating a single-emission approximation of the cross section. The parton branching at amplitude level was designed around the soft gluon evolution algorithm presented earlier, and included the hard-collinear contributions by extending the dipole structure of the leading order soft evolution. Work is underway to extend this algorithm to the next order, including an expansion around the colour-diagonal contributions [26] corresponding to the d' -expansions advocated in [27].

In this work we focus on extending the parton branching in amplitude level algorithms to account for more than singly-unresolved limits, concentrating on corrections due to iterating the emission of two or more simultaneously unresolved partons. We work at a finite number of colours, and include the full spin dependence aiming to establish factorization at the level of the ‘density operator’, *i.e.* the amplitude and its conjugate, for which we can devise the definition of splitting kernels. These encompass all enhanced configurations of both soft, collinear, or any combination of unresolved limits. We also highlight the connection of the underlying power counting to the way recoil is distributed and how

kinematics are parametrized.

This paper is structured as follows: In Sec. 2 we will outline the general framework in which we establish the iterative factorization of the density operator. We will highlight the connection to the light-cone gauge we employed, as well as the distribution of recoil of emissions among the hard jet axes, which allows us to establish a diagrammatic framework in which the splitting kernels can be calculated. After the projection onto different collinearly enhanced contributions, which we refer to as partitioning, we will be able to establish a systematic power counting and a final calculational recipe for the emission operators. In Sec. 3, the partitioning is set up in an algorithmic manner and is suited to be carried out to an in principle arbitrary number of emissions from a hard process.

In Sec. 4 we detail one particular instance of a suitable momentum mapping and discuss its properties in the unresolved limit, as well as how it can be used to construct an actual parton branching algorithm concerning the real emission contributions. In combination with singling out collinear limits, and the proper choice of a backward vector n , we can determine the splitting kernels. We discuss a few examples in Sec. 5, also addressing how the underlying amplitude can be taken on-shell from the final state considered (before emissions are added) and which power suppressed effects we neglect in doing so.

In Sec. 6 we conclude by discussing applications of our formalism, and how our framework can be generalized to the case of virtual corrections. The determination of a full set of QCD splitting kernels is devoted to a future publication, however we do discuss several examples, as well as the possibility to link our formalism to a partitioning of the known singular behaviour of two emissions, and a systematic removal of overlap between the soft and collinear limits. A number of technical details and material for future reference is devoted to several appendices, which do not need to be considered to understand the main findings of our current work.

2 Construction of splitting kernels

While traditional parton branching algorithms use probabilistic paradigms based on the factorization of cross sections, our aim is to address parton branching algorithms at the amplitude level, as recently theoretically developed and implemented in [13, 21, 24, 27]. Only within such an approach is it possible to iteratively approximate amplitudes with many legs and to derive Markovian algorithms which then might be able to perform multiple emissions at the probabilistic level; iterating approximations of a fixed-order cross section will yield the right singularity structure, but otherwise not guarantee the right resummation properties. In the present work, we focus on the systematic construction of real emission splitting kernels within such a branching algorithm, addressing the simultaneous emission of more than one unresolved parton. The goal of the present work is to not perform this specifically in one unresolved limit, but to obtain a combination of splitting operators which smoothly cover the different singular limits. Some aspects of virtual corrections have recently also been addressed in [26] and will be combined with the present effort in future work. We can of course use our results to obtain splitting kernels which can also serve as subtraction terms in fixed-order corrections, though this is not our primary goal.

To set the notation, we consider scattering amplitudes $|\mathcal{M}\rangle$ to be vectors in colour and spin space (see [28] for an outline of this formalism), from which cross sections originate as

$$\sigma[u] = \sum_n \int \text{Tr} [|\mathcal{M}(1, \dots, n)\rangle \langle \mathcal{M}(1, \dots, n)|] u(1, \dots, n) d\phi(1, \dots, n|Q) , \quad (2.1)$$

where $d\phi(1, \dots, n|Q)$ commonly refers to the n -parton phase space given a total momentum Q and the arguments of the amplitude vector and phase space measure refer to both parton momenta, as well as other degrees of freedom needed to identify a particular final state. u is a generic observable with the same convention on arguments understood, *i.e.* $u(1, \dots, n) = u(p_1, \dots, p_n)$ for specific momenta. In the present work we also only consider massless partons. The trace in Eq. (2.1) refers to summing over the colour and spin degrees of freedom in the amplitude and its conjugate, seen as an operator in colour and spin space, the cross section density operator

$$\mathbf{A}_n = |\mathcal{M}(1, \dots, n)\rangle \langle \mathcal{M}(1, \dots, n)| , \quad (2.2)$$

which will be the central object of our investigation. The trace can typically be expressed using the completeness of external wave functions, and we shall decompose the respective numerator of a cut propagator in such a way that we can find a similar decomposition of internal lines, with suitably parametrized kinematics. With this in mind, we will then formulate a diagrammatic construction of the relevant splitting kernels, directly involving a power counting to identify the leading contributions of interest. Working in a physical gauge with gauge fixing $C^a = n \cdot A^a$, $n^2 = 0$, we in particular note that we can express the propagator numerators for cut gluon lines of on-shell momentum q as

$$d_{\mu\nu}(q) = -\eta^{\mu\nu} + \frac{n^\mu q^\nu + n^\nu q^\mu}{n \cdot q} , \quad (2.3)$$

such that we can use

$$d_{\mu\nu}(q) = d_{\mu\rho}(q) P^{\rho\sigma}(p) d_{\sigma\nu}(q), \quad P^{\rho\sigma}(p) = d^{\rho\sigma}(p) , \quad (2.4)$$

which holds for $q^2 = 0$, while for quark lines we can employ

$$\not{q} = \sqrt{\frac{n \cdot q}{n \cdot p}} \frac{n \cdot p}{n \cdot q} \not{q} \not{P}(p) \not{q} \frac{n \cdot p}{n \cdot q} \sqrt{\frac{n \cdot q}{n \cdot p}}, \quad \not{P}(p) = \frac{\not{p}}{2n \cdot p} , \quad (2.5)$$

where p is the forward component we associate to the external momentum q in a decomposition

$$q^\mu = \alpha p^\mu + \beta n^\mu + q_\perp^\mu , \quad q_\perp \cdot n = q_\perp \cdot p = 0 . \quad (2.6)$$

The reason for the awkward decomposition of the quark numerator as in Eq. (2.5) is to associate the square-root factors with the vertex the quark couples into (or leave it as an explicit factor if such a coupling is not considered), while the factors $n \cdot p/n \cdot q$ provide a convenient normalization in the power counting such that quark and gluon lines have a uniform scaling. The role of soft quarks in the factorization can then be tracked separately

from more general considerations on factorization of the amplitude. This is discussed in Sec. 2.1. In a more abstract notation we thus define

$$\mathbf{P}(q) \equiv \begin{cases} P^{\rho\sigma}(p) = d^{\rho\sigma}(p), & \text{for gluons,} \\ \not{p}(p) = \frac{\not{p}}{2n \cdot p}, & \text{for quarks,} \end{cases} \quad (2.7)$$

where it should always be clear which forward momentum p we associate to a certain external momentum q , subject to a decomposition of the density operator into different collinearly singular configurations to be discussed in Sec. 2.2. Moreover, we can use polarisation sums to represent these operators, *i.e.*

$$d^{\mu\nu}(p) = \epsilon_+^\mu(p, n)\epsilon_-^\nu(p, n) + (\mu \leftrightarrow \nu), \quad (2.8)$$

$$\not{p} = \sum_\lambda u_\lambda(n)\bar{u}_\lambda(n), \quad (2.9)$$

with

$$\epsilon_\pm^2 = 0, \quad \epsilon_\pm \cdot \epsilon_\mp = -1, \quad \epsilon_\pm \cdot p = \epsilon_\pm \cdot n = 0. \quad (2.10)$$

Also note that for internal lines carrying a sum of momenta, we can decompose the respective numerators via

$$d^{\mu\nu}(q_I + q_J) = \frac{n \cdot q_I}{n \cdot q_I + n \cdot q_J} \times d^{\mu\nu}(q_I) + (I \leftrightarrow J), \quad (2.11)$$

$$\not{q}_I + \not{q}_J = \sqrt{\frac{n \cdot q_I}{n \cdot p_i}} \left(\frac{n \cdot p_i}{n \cdot q_I} \not{q}_I \right) \sqrt{\frac{n \cdot q_I}{n \cdot p_i}} + (I \leftrightarrow J),$$

where q_I and q_J themselves can be sums of momenta in distinct sets of partons I and J . Moreover, the square root factors in the second line are of the same use as in Eq. (2.5). Similarly, we can decompose the three-gluon vertex due to its linearity in the momenta, *i.e.*

$$\text{Diagrammatic equation (2.12)} \quad (2.12)$$

If now all of the partons in the set J become soft, then only the first terms in Eq. (2.11) and Eq. (2.12) will contribute in a leading soft limit. This paves the way to establish a universal set of rules to decompose the cross section with many external, unresolved, legs as follows: Using Eq. (2.7), we can write

$$\text{Tr}[\mathbf{A}_n] = \text{Tr}_c \left[\tilde{\mathbf{A}}_n \times \mathbf{P}_n \right], \quad (2.13)$$

where Tr_c now solely refers to a trace in colour space, $\tilde{\mathbf{A}}_n$ is the density operator obtained from \mathbf{A}_n by removing all external wave functions. The sum over external polarisations is implicitly carried out by associating the normalized completeness relations of external wave functions to each external line, *i.e.* applying a factor $d^{\mu\nu}(q)$ for each external gluon

line and a factor of $(q \cdot n \cdot p/n \cdot q) \times \sqrt{n \cdot q/n \cdot p}$ to each external fermion line, together with the insertion of the respective operator \mathbf{P} . This setup allows us to treat internal and external lines for quarks and gluons alike on the same footing and devise universal power counting rules in the following parts of this section. Those will eventually be used to dissect numerator structures of emission amplitudes in terms of their soft or collinear scaling and allows for a precise association of which parts of an amplitude contribute in singular limits at a given power. The results of these considerations for one and two emissions are given in Sec. 5.3 and Sec. 5.4 respectively. Also note that it is in principle possible to include a polarized measurement into the definition of the \mathbf{P} operator by appropriately restricting the sums of external wave functions, though this is beyond the scope of the present work.

Starting from the amplitude, we consider a certain subset of diagrams contributing to additional emissions from a general amplitude $|\mathcal{M}\rangle$, which we consider to be a vector in spin and colour space. In particular, we are interested in the emission of several, $k \geq 1$ additional particles, for which we consider the diagrams factorizing in an $(n+k)$ -particle amplitude in terms of emission diagrams and an underlying, n -particle hard amplitude as

$$|\mathcal{M}_{n+k}(1, \dots, n+k)\rangle = \sum_{p=1}^k \sum_{r \in S_{n,p,k}} \mathbf{Sp}_{(r_{11}|\dots|r_{1\ell_1})} \dots \mathbf{Sp}_{(r_{p1}|\dots|r_{p\ell_p})} |\tilde{\mathcal{M}}_n(1, \dots, (r_{11}|\dots|r_{1\ell_1}), \dots, (r_{p1}|\dots|r_{p\ell_p}), \dots, n+k)\rangle, \quad (2.14)$$

or in a diagrammatic representation

$$\quad (2.15)$$

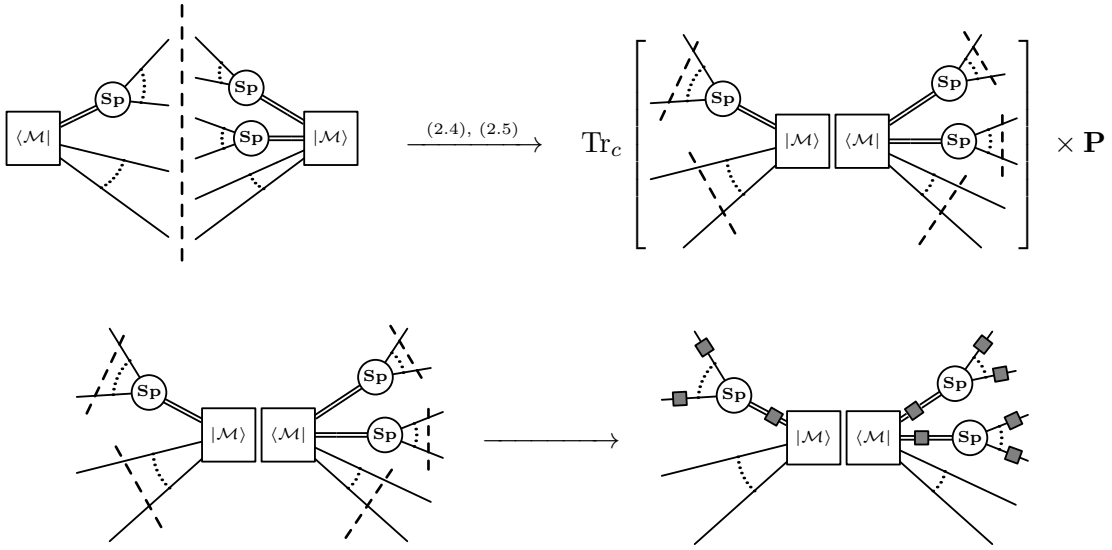
$S_{n,p,k}$ is the set of possible splitting assignments involving p emitters and k emissions out of $n+k$ external particles, and

$$(r_{i1}|\dots|r_{i\ell_i}) = r_{i1} + \dots + r_{i\ell_i} \quad (2.16)$$

are the off-shell momenta of the branching internal lines, where each of the r_{ik} denotes a certain external momentum q_j involved in the splitting process. We are interested in the unresolved limits of the k emitted partons, in which all of the off-shell momenta $(r_{i1}|\dots|r_{i\ell_i})$ will become on-shell and the splitting amplitudes are expected to factorize in a universal manner, within which the underlying amplitude $\tilde{\mathcal{M}}$ in fact becomes an on-shell amplitude. The leading singular behaviour of the cross section is then obtained by considering the square of the amplitude, or equivalently a density-operator type object, such that none of the partons participating in an unresolved limit are connected to an internal line. To be more precise we can write

$$\begin{aligned}
|\mathcal{M}_{n+k}(1, \dots, n+k)\rangle \langle \mathcal{M}_{n+k}(1, \dots, n+k)| = & \\
\sum_{p=1}^k \sum_{\bar{p}=1}^k \sum_{r \in S_{n,p,k}} \sum_{\bar{r} \in S_{n,\bar{p},k}} \mathbf{Sp}_{(r_1)} \dots \mathbf{Sp}_{(r_p)} |\mathcal{M}_n(1, \dots, (r_1), \dots, (r_p), \dots, n+k)\rangle & \\
\langle \mathcal{M}_n(1, \dots, (\bar{r}_1), \dots, (\bar{r}_{\bar{p}}), \dots, n+k) | \mathbf{Sp}_{(\bar{r}_1)}^\dagger \dots \mathbf{Sp}_{(\bar{r}_{\bar{p}})}^\dagger \times \hat{\Delta}_{\bar{r}}^r + & \\
& \text{(subleading)} \quad (2.17)
\end{aligned}$$

where we have introduced short-hands for the splitting labels, $(r_i) = (r_{i1} | \dots | r_{i\ell_i})$ and similar. The tensor $\hat{\Delta}_{\bar{r}}^r$ ensures that we only include those diagram topologies which give rise to leading singularities. See Appendix D for its explicit construction. This extraction of leading singularities is valid as long as we work in a physical gauge. The diagrammatic representation of one such leading singular contribution to the density operator is:



This procedure needs to be understood as follows: First we apply our identities to decompose the square of the matrix element into the operators \mathbf{P} and a set of cut lines, where a dashed cut line indicates a use of

$$\not{q} \frac{n \cdot p}{n \cdot q} \quad \text{or} \quad d^{\mu\nu}(q)$$

for each on-shell external quark or gluon line, respectively. Internal lines carrying a sum of different momenta will be decomposed as indicated by Eqs. (2.11), and a factor of $\sqrt{n \cdot q_a / n \cdot p_a} \sqrt{n \cdot q_b / n \cdot p_b}$ will be applied to each quark-gluon vertex with incoming fermion momentum q_a (with forward momentum p_a) and each outgoing fermion momentum q_b (with forward momentum p_b). We then carry out the decomposition of an amplitude's numerator in terms of its forward (along jet directions p_i^μ), backward (along the gauge vector n^μ) and transverse (n_\perp^μ) components, indicated by the grey boxes in the last diagram of the workflow depicted above. Forward directions are chosen with respect to jets emerging from a hard interaction, such that we can properly trace collinear and/or soft configurations through several emitted partons in the diagram, as well as iterating

kernels describing a particular unresolved configuration, however a universal factorization onto an on-shell density operator will generally only happen in very specific configurations of unresolved emissions. To this extend we shall re-interpret Eq. (2.17) by writing it as a sum over different topologies of diagrams in the amplitude and conjugate amplitude, which we label ρ and $\bar{\rho}$, respectively:

$$\tilde{\mathbf{A}}_{n+k} = \sum_{\rho, \bar{\rho}} \widetilde{\mathbf{S}}\mathbf{p}_{n, \rho}^{(k)} \mathbf{B}_{n, n+k, \rho, \bar{\rho}} \widetilde{\mathbf{S}}\mathbf{p}_{n, \bar{\rho}}^{(k), \dagger} , \quad (2.18)$$

where $\mathbf{B}_{n, n+k, \rho, \bar{\rho}}$ is obtained by removing the splitting diagrams labelled by ρ and $\bar{\rho}$, and still constitutes the outer product of two amplitudes with different compositions of on-shell and off-shell external lines.

Crucially, the off-shell lines at which we will attempt to factor off emission subdiagrams will be nearly on-shell in the unresolved configurations, yet we need to restore overall energy momentum conservation. In our approach we choose to do this by a global Lorentz transformation combined with a scaling of each of the final state momenta, such that momenta q_i after emission, and with momentum conservation maintained, $\sum_i q_i = Q$ are parametrised as

$$q_i^\mu = \frac{1}{\hat{\alpha}} \Lambda^\mu{}_\nu \hat{q}_i^\nu , \quad (2.19)$$

where the \hat{q}_i are decomposed into the jet directions and do not obey momentum conservation, $\sum_i \hat{q}_i = Q + N$. The scaling factor $\hat{\alpha}$ then simply encodes the correction of the different mass shells $(Q+N)^2$ and Q^2 . The recoil momentum N can thus easily be absorbed through the Lorentz transformation. The advantage of such an approach is that recoil effects are now completely removed from considerations about factorizing the amplitude, as we can use Lorentz invariance and the known mass dimension of the amplitude to remove this effect. More precisely,

$$|\mathcal{M}(q_1, \dots, q_n)\rangle = \frac{1}{\hat{\alpha}^{2n-4}} |\mathcal{M}(\hat{q}_1, \dots, \hat{q}_n)\rangle . \quad (2.20)$$

In the following we will, unless stated otherwise, therefore treat the transformed and untransformed momenta as equivalent. Notice that for additional, massive particles involved, we can easily extend such a recoil scheme which will not change the argument given here. Notably, when working in a physical gauge, as we choose below, the gauge vector n will also have to be transformed by the recoil prescription in order for the argument to stay valid. We will link this to how the recoil transformation should be iterated in Sec. 2.2.

An expansion around a certain limit in which the off-shell lines become on-shell in Eq. (2.18) is possible only if we can expose this particular limit by a weighting factor, ensuring that no other singular limit can contribute by virtue of either the weighting (or partitioning) factor we introduce or the physical gauge we choose. We therefore write Eq. (2.18) as

$$\tilde{\mathbf{A}}_{n+k} = \sum_{\rho} \left[\sum_{\lambda} \left(\frac{w_{\rho, \lambda; \rho}}{w_{\rho, \lambda}} \widetilde{\mathbf{S}}\mathbf{p}_{n, \rho}^{(k)} \mathbf{B}_{n, n+k, \rho, \lambda} \widetilde{\mathbf{S}}\mathbf{p}_{n, \lambda}^{(k), \dagger} + \frac{w_{\lambda, \rho; \rho}}{w_{\lambda, \rho}} \widetilde{\mathbf{S}}\mathbf{p}_{n, \lambda}^{(k)} \mathbf{B}_{n, n+k, \lambda, \rho} \widetilde{\mathbf{S}}\mathbf{p}_{n, \rho}^{(k), \dagger} \right) + \right.$$

$$\left. \sum_{\lambda \neq \rho} \sum_{\sigma \neq \rho} \frac{w_{\sigma, \lambda; \rho} \widetilde{\mathbf{Sp}}_{n, \sigma}^{(k)}}{w_{\sigma, \lambda}} \mathbf{B}_{n, n+k, \sigma, \lambda} \widetilde{\mathbf{Sp}}_{n, \lambda}^{(k), \dagger} \right], \quad (2.21)$$

with $w_{\rho, \bar{\rho}} = \sum_{\sigma} w_{\rho, \bar{\rho}; \sigma}$ and where $w_{\rho, \bar{\rho}; \sigma}$ ensures that a diagram with propagator structures identified by ρ and $\bar{\rho}$ contains a collinear enhancement solely as dictated by the topology σ , but not by those identified through ρ and $\bar{\rho}$ (though all of these might contain common configurations of collinear enhancement). An index ρ can be visualized as part of a set of distinct emission patterns, which can in turn be mapped to ordered tuples of the set of all partons involved in an $(n+k)$ -splitting. This procedure will allow us to uniquely identify one parametrization of the external momenta in terms of forward and backward directions which we can then use to set up a systematic power counting in each singular limit.

As an example to illustrate the contributions in Eq. (2.21), we examine it for fixed $\rho = (ijk)$, meaning a splitting with a hard line i and two sequential emissions j and k off of it. Then the first line in Eq. (2.21) represents all two emission topologies containing this emission pattern, such as the self energy $E^{(1)}$ for $\lambda = \rho$ or topology $B^{(1)}$ for $\lambda = (ij)(lk)$ and their conjugates (see App. C for a list of topologies). The third term represents all topologies that do not contain this emission pattern, such as the X -topology. Each contribution is multiplied by their respective weighting factor which cancels all singular factors not belonging to the (ijk) -collinear sector. These are precisely the partitioning factors of Sec. 3. In this way of a decomposition, we are able to collect all possible contributions to a specific splitting pattern. The collection of such terms for fixed ρ is what we call *splitting kernels* which are defined in Sec. 5.

2.1 Decomposition of amplitudes in a physical gauge

Once we have identified a certain splitting process by the emission subdiagrams contributing in the amplitude factor, *i.e.* one term of fixed ρ in Eq. (2.21), we decompose all of the momenta involved in each splitting (r_i) as

$$r_{ik}^{\mu} = z_{ik} p_i^{\mu} + \frac{p_{\perp, ik}^2}{z_{ik} 2p_i \cdot n} n^{\mu} + k_{\perp, ik}^{\mu}, \quad (2.22)$$

where $k_{\perp, ik}^2 = -p_{\perp, ik}^2$, $p_i \cdot k_{\perp, ik} = n \cdot k_{\perp, ik} = 0$ and p_i is the momentum of a progenitor of the splitting. An off-shell internal line I within a splitting subdiagram (r_i) in the amplitude carries momenta of the form

$$q_I^{\mu} = \sum_{k \in I} r_{ik}^{\mu} = z_I p_i^{\mu} + \frac{S_I + p_{\perp, I}^2}{z_I 2p_i \cdot n} n^{\mu} + k_{\perp, I}^{\mu}, \quad (2.23)$$

where $q_I^2 = S_I > 0$ and the transverse components as well as momentum fractions are additive

$$k_{\perp, I}^{\mu} = \sum_{k \in I} k_{\perp, ik}^{\mu}, \quad z_I = \sum_{k \in I} z_{ik}, \quad (2.24)$$

while

$$S_I = \left(\sum_{k \in I} z_{ik} \right) \sum_{l \in I} \frac{p_{\perp, il}^2}{z_{il}} + \sum_{k, l \in I} k_{\perp, ik} \cdot k_{\perp, il}, \quad p_{\perp, I}^2 = \left(\sum_{k \in I} k_{\perp, ik}^{\mu} \right)^2, \quad (2.25)$$

such that

$$\beta_I \equiv \frac{S_I + p_{\perp,I}^2}{2z_I p_i \cdot n} = \frac{1}{2p_i \cdot n} \sum_{k \in I} \frac{p_{\perp,ik}^2}{z_{ik}}, \quad (2.26)$$

consistent with momentum conservation. Notice that, if all lines combining into I are collinear w.r.t. p_i , meaning $p_{\perp,ik} \rightarrow \lambda p_{\perp,ik}$, we obtain $S_I \sim \lambda^2$; if all lines are soft, $p_{\perp,ik} \rightarrow \lambda p_{\perp,ik}$ and $z_{ik} \rightarrow \lambda z_{ik}$, we obtain the same. However, if one line k is hard collinear in the sense that it has an $z_{ik} = \mathcal{O}(1)$, we find $S_I \sim \lambda^2$ only in the limit of all lines becoming collinear, while $S_I \sim \lambda$ in the combined soft/collinear limit. For the backward component this implies that it is $\mathcal{O}(\lambda)$ for all soft, or a soft/collinear combination, and $\mathcal{O}(\lambda^2)$ for an all-collinear configuration. An overview of the line- and vertex-scalings in all possible collinear and soft settings is shown in Sec. 2.5.

We can use Eq. (2.23) for decomposing the scaled fermion numerators $(n \cdot p_i / n \cdot q_I) \not{q}_I$ as

$$\text{---} \square \text{---} = \not{p}_i, \quad (2.27a)$$

$$\text{---} \blacksquare \text{---} = \frac{S_I + p_{\perp,I}^2}{2z_I^2 p_i \cdot n} \not{p} = \frac{1}{z_I} \sum_{k \in I} \frac{-k_{\perp,ik}^2}{z_{ik} 2p_i \cdot n} \not{p}, \quad (2.27b)$$

$$\text{---} \square \text{---} = \frac{\not{k}_{\perp,I}}{z_I} = \frac{\sum_{k \in I} \not{k}_{\perp,ik}}{\sum_{k \in I} z_{ik}}, \quad (2.27c)$$

and for gluon lines $d^{\mu\nu}(q_I)$ as

$$\text{---} \square \text{---} = d^{\mu\nu}(p_i), \quad (2.28a)$$

$$\text{---} \blacksquare \text{---} = \frac{S_I + p_{\perp,I}^2}{(z_I p_i \cdot n)^2} n^\mu n^\nu = \frac{1}{z_I} \sum_{k \in I} \frac{-k_{\perp,ik}^2}{z_{ik} (p_i \cdot n)^2} n^\mu n^\nu, \quad (2.28b)$$

$$\text{---} \square \text{---} = \frac{k_{\perp,I}^\mu n^\nu + n^\mu k_{\perp,I}^\nu}{z_I p_i \cdot n} = \frac{\sum_{k \in I} k_{\perp,ik}^\mu n^\nu + \sum_{k \in I} n^\mu k_{\perp,ik}^\nu}{\sum_{k \in I} z_{ik} p_i \cdot n}. \quad (2.28c)$$

These decompositions hold both for the numerators we obtain from the sum over external wave functions, and internal lines. Comparing Eq. (2.27) with Eq. (2.28) shows that the components in these decompositions give the same soft and collinear scaling behaviour for quarks and gluons. To this extent we can 'colour' all internal lines in the amplitude and the conjugate amplitude, as well as the external lines by the different contributions in the decomposition above. Note that it suffices both for external on-shell gluon and quark lines to use the projectors with only the forward momentum component p_i as an argument, due to

$$\not{p}_{ik} \frac{\not{p}}{2n \cdot p_i} \not{p}_{ik} = z_{ik} \not{p}_{ik}, \quad (2.29a)$$

$$d^{\mu\rho}(r_{ik}) d_{\rho\sigma}(p_i) d^{\sigma\nu}(r_{ik}) = d^{\mu\nu}(r_{ik}). \quad (2.29b)$$

Moreover, we find the following rules for connecting on-shell lines via the projectors, *viz.*

$$\mathbf{P}(p_i) \text{---} \blacksquare \text{---} \circ = 0, \quad (2.30a)$$

$$\circ \text{---} \square \text{---} \mathbf{P}(p_i) \text{---} \square \text{---} \circ = \circ \text{---} \square \text{---} \circ, \quad (2.30b)$$

$$\circ \text{---} \sqcup \text{---} \mathbf{P}(p_i) \text{---} \sqcup \text{---} \circ = \circ \text{---} \blacksquare \text{---} \circ, \quad (2.30c)$$

$$\circ \text{---} \sqcup \text{---} \mathbf{P}(p_i) \text{---} \square \text{---} \circ + \circ \text{---} \square \text{---} \mathbf{P}(p_i) \text{---} \sqcup \text{---} \circ = \circ \text{---} \sqcup \text{---} \circ, \quad (2.30d)$$

which hold both for quarks and gluons. Due to Eq. (2.30a) and Eq. (2.30c), we note that the backwards (n) components on external lines do not need to be taken into account in the decomposition of an amplitude. Via these rules, we are able to translate our density operator-like discussion to the one of cut diagrams or vice versa.

Let us first discuss the vertex structures coupling these different internal lines. We find that, making use of the fact that $n_\mu d^{\mu\nu} = 0$, the quark gluon vertex and three gluon vertex can effectively be decomposed into two components depending only on the longitudinal and only on the transverse components,

$$\begin{array}{c} \text{Diagram 1: A vertex with a double line (||) and a wavy line (k) meeting at a central point. Two external lines (j and i) are attached to the double line.} \\ \text{Diagram 2: A vertex with a double line (||) and a wavy line (z_k p_k) meeting at a central point. Two external lines (z_j p_j and z_i p_i) are attached to the double line.} \end{array} = \sqrt{z_i z_j} \quad (2.31a)$$

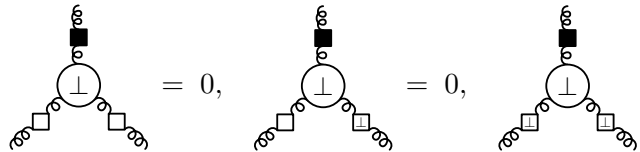
$$\begin{array}{c} \text{Diagram 1: A vertex with a double line (||) and a wavy line (i) meeting at a central point. Two external wavy lines (k and j) are attached to the double line.} \\ \text{Diagram 2: A vertex with a double line (||) and a wavy line (z_i p_i) meeting at a central point. Two external wavy lines (z_k p_k and z_j p_j) are attached to the double line.} \end{array} = \quad (2.31b)$$

$$\begin{array}{c} \text{Diagram 1: A vertex with a double line (⊥) and a wavy line (i) meeting at a central point. Two external wavy lines (k and j) are attached to the double line.} \\ \text{Diagram 2: A vertex with a double line (⊥) and a wavy line (k_{\perp i}) meeting at a central point. Two external wavy lines (k_{\perp k} and k_{\perp j}) are attached to the double line.} \end{array} = \quad (2.31c)$$

We also find that certain combinations of lines always vanish, irrespective of the progenitor momentum and/or the off-shellness of the lines. In particular this applies to the cases in which more than one line with a black square connects to a vertex, indicating that a backward component can only propagate upon exchanging at least some transverse or longitudinal momentum with another parton,

$$\begin{array}{c} \text{Diagram 1: A vertex with three black squares (blacksquare) and one white square (square).} \\ \text{Diagram 2: A vertex with two black squares (blacksquare) and two white squares (square).} \\ \text{Diagram 3: A vertex with one black square (blacksquare) and three white squares (square).} \end{array} = 0, \quad (2.32)$$

both for quark and gluon insertions. The following vertices also vanish but only in the gluon case:



$$= 0, \quad = 0, \quad = 0. \quad (2.33)$$

Further simplifications occur if all lines which are coupled together share the same forward direction; in this case we also have that vertices coupling three forward components vanish identically, if the participating momenta have been decomposed with respect to the same forward direction p_i .

2.2 Decomposing around singular limits

Let us first focus on those terms in Eq. (2.21) for which we can uniquely assign a splitting configuration to the diagram in the amplitude or conjugate amplitude, *i.e.* the terms in the first line of Eq. (2.21).

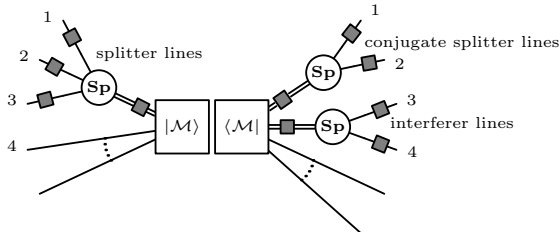


Figure 1: Illustration of the terminology used to describe the different parts of a splitting topology.

To illustrate our terminology let us focus on a topology like the one depicted in Fig. 1, where we have identified a certain set of splitting amplitudes in the amplitude side (the left hand part of the diagram) which we refer to as ‘splitter lines’, and possibly different combinations of splitting amplitudes in the conjugate (right hand) side of the density operator diagram. Splittings of this kind, which solely involve momenta which are attached to a single splitting blob on the left hand side are referred to as ‘conjugate splitting lines’, while otherwise we refer to them as ‘interferer lines’. Fig. 1 contains an example of our notation.

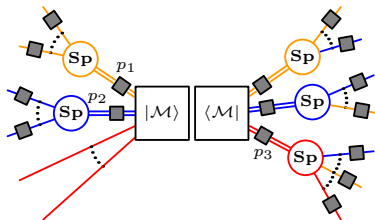


Figure 2: Illustration of the collinear directions

Our power counting in the singular limits will be organized around the assumption that we can prevent those momenta attached to a splitter line from developing collinear

singularities with respect to any other than their progenitor direction. This can be imposed by the restrictions of a certain observable which *e.g.* is requiring a fixed number of jets, or by an algorithmic construction of a ‘partitioning’, an example of which we will outline in Sec. 3 for one and two emissions. We illustrate this idea in Fig. 2, where double lines represent different hard directions and the colours signify which lines are connected in a corresponding cut-diagram. Using the weighting factors $\omega_{\rho\bar{\rho};\sigma}$ of Eq. (2.21), one can extract the collinear behaviour to some subset of hard lines, *e.g.* the yellow ones in Fig. 2, via the choice of the respective splitting configuration σ . For a fixed-order analysis such a partitioning can serve as the basis to construct subtraction terms, or we can view it in an integrated way to obtain evolution kernels for a full-fledged parton branching algorithm. A further assumption we make is that each ‘splitter line’ has one hard momentum flowing through it, and that each ‘conjugate splitter’ and ‘interferer line’ do so as well. We therefore consider to decompose all momenta which are assigned to the ‘splitter’ lines to be decomposed with one progenitor momentum per splitter line, both in the amplitude as well as its conjugate, *i.e.* we shall *not* decompose the momenta attaching to interferer lines in terms of the hard momentum defining the interferer direction. Conversely, the hard momentum in the interferer direction shall be parametrized taking into account the interferer direction. Couplings between different collinear sectors, hence, only need to be considered for conjugate splitter lines, or for vertices coupling lines from different splitter lines.

Let us stress that for conjugate splitter or interferer lines which have internal lines from different collinear sectors we can employ Eq. (2.11) and Eq. (2.12) to decouple the different sectors. Such a line, say one carrying $q_I + q_J$, will then split into one with a numerator according to q_I and one according to q_J , and the net enhancement to be studied is the partitioning’s effect along with the combination

$$\frac{z_I}{z_I + z_J(n \cdot p_j/n \cdot p_i)} \times \frac{1}{(q_I + q_J)^2} \times (\text{partitioning/observable}) ,$$

and a similar one for exchanging I with J . If the partitioning and/or the observable thus guarantees that there will not be a singularity arising from q_I becoming collinear to q_J , the above configuration is finite also in the limit of q_I becoming soft, $z_I \rightarrow 0$ as long as a hard momentum flow asserts $z_J = \mathcal{O}(1)$. Notice that we still might need to consider those contributions in expanding to a certain power of λ , however in the present work we shall only be concerned with extracting the singular behaviour.

The contributions entering in the second line of Eq. (2.21) are slightly more complicated in the sense that there is no one-to-one correspondence between a collinear sector and a sub-diagram. However, since the partitioning factor $w_{\lambda,\sigma;\rho}$ guarantees that there will only be a collinear enhancement as dictated by the topology ρ and this topology being excluded from the ones summed over, emission lines in λ and σ are forced to become soft for the contribution to be enhanced. Then, our discussion on the decomposition of internal lines applies, and the coupling within common collinear sectors applies otherwise. Therefore, we can think of these contributions consisting of interferer lines in both the amplitude and conjugate amplitude.

2.3 Iterating the recoil transformation

Our discussion on the power counting can also be applied to iterating emission kernels in a Markovian manner, as long as we make sure that the recoil transformation does not change the general decomposition. To be precise, we consider, in a $k + 1$ st emission step, a decomposition¹

$$q_{(k+1)}^\mu = \frac{1}{\hat{\alpha}_{(k+1)}} (\Lambda_{(k+1)})^\mu{}_\nu \left(z_{(k+1)} p_{(k)}^\nu + \beta_{(k+1)} n_{(k+1)}^\nu + k_{\perp, (k+1)}^\nu \right), \quad (2.34)$$

where the forward direction has been changed due to the previous emission and itself admits a decomposition (we do here not distinguish what branching it belonged to)

$$p_{(k)}^\mu = \frac{1}{\hat{\alpha}_{(k)}} (\Lambda_{(k)})^\mu{}_\nu \left(z_{(k)} p_{(k-1)}^\nu + \beta_{(k)} n_{(k)}^\nu + k_{\perp, (k)}^\nu \right). \quad (2.35)$$

It is therefore tempting to redefine the backward direction as

$$n_{(k+1)}^\mu = \frac{1}{\hat{\alpha}_{(k)}} (\Lambda_{(k)})^\mu{}_\nu n_{(k)}^\nu, \quad (2.36)$$

which leads to

$$q_{(k+1)}^\mu = \frac{1}{\hat{\alpha}_{(k+1)} \hat{\alpha}_{(k)}} (\Lambda_{(k+1)})^\mu{}_\nu (\Lambda_{(k)})^\nu{}_\rho \left[z_{(k+1)} z_{(k)} p_{(k-1)}^\rho + (\beta_{(k+1)} + z_{(k+1)} \beta_{(k)}) n_{(k)}^\rho + z_{(k+1)} k_{\perp, (k)}^\rho + \hat{\alpha}_{(k)} (\Lambda_{(k)}^{-1})^\rho{}_\sigma k_{\perp, (k+1)}^\sigma \right], \quad (2.37)$$

However, this might actually not be sufficient to guarantee that the mapping iterates the momentum parametrization in the way that would not change our general power counting arguments. In particular this happens if, for an emission off of a hard line, we allow a transverse component assigned through the emission process. In this case, iterating the above to the second emission will generate a transverse momentum which, despite being still orthogonal to the backward direction chosen initially by virtue of Eq. (2.36), will not be orthogonal to the forward direction anymore, *i.e.*

$$p_{(k-1)} \cdot (\Lambda_{(k)}^{-1} k_{\perp, (k+1)}) = -\frac{\hat{\alpha}_{(k)}}{z_{(k)}} k_{\perp, (k)} \cdot (\Lambda_{(k)}^{-1} k_{\perp, (k+1)}) \neq 0, \quad (2.38)$$

potentially introducing azimuthal correlations between the emissions and spoiling our power counting arguments. As already mentioned, this can only be avoided by not introducing transverse momentum components for hard lines in the first place, which we will call “unbalanced mapping”, or by parametrizing two or more emissions in one step. In Sec. 4, we explore mappings of this kind in detail. We believe that this discussion intimately connects to the findings one of the authors and others have been highlighting in [5, 19–21]. We therefore do not limit the discussion of our mappings to include balance of transverse recoil, and leave this open to an algorithmic choice which can, however, crucially impact the accuracy of algorithms build on top of our calculations. Similar remarks

¹We suppress the label for the collinear sector in this discussion.

apply to the ordering variable, which should then be chosen, in line with the partitioning which has been used to separate different collinear sectors, to not spill the configurations we have been discussing within our power counting arguments. We also stress that the above way of re-defining the backward (gauge) vector is crucial to establish that the recoil transformation factors out of the amplitude in the same homogeneous way as discussed earlier, since the amplitude additionally depends on the backward direction n . In the presence of non-coloured (or coloured, massive) objects, the recoil scheme above can easily be generalized and still be implemented by virtue of a single Lorentz transformation; however the amplitude will not easily satisfy a scaling property since the massive momenta cannot be rescaled in order to remain on their definite, non-vanishing mass shell. However, in the singular regions, the scaling factor $\hat{\alpha}$ will in any case tend to unity such that no additional complication should arise in this case.

Depending on how the transverse recoil has been chosen, different diagrams then contribute after decomposing the internal lines into the Sudakov decomposition and applying the vertex rules above. We will highlight a few examples below, and defer a more detailed analysis to Sec. 5, where we also discuss the relation to splitting functions and the soft limit, as well as the strategy employed for the dipole subtraction terms in [28].

2.4 Local backward direction

Provided we have decomposed the momenta into a component towards a certain hard direction, but with an arbitrary backward direction,

$$q^\mu = \tilde{z} p^\mu + \frac{\tilde{p}_\perp^2}{\tilde{z} 2p \cdot \tilde{n}} \tilde{n}^\mu + \tilde{k}_\perp, \quad (2.39)$$

with $\tilde{k}_\perp \cdot p = \tilde{k}_\perp \cdot \tilde{n} = 0$, $\tilde{k}_\perp^2 = -\tilde{p}_\perp^2$ and $p \cdot \tilde{n} > 0$ as usual, we can uniquely relate this to our global parametrization with respect to p , n and an appropriate transverse momentum k_\perp as

$$p_\perp^2 = \tilde{p}_\perp^2 R, \quad z = \tilde{z} R, \quad R = 1 + \frac{1}{\tilde{z}} \frac{n \cdot \tilde{k}_\perp}{n \cdot p} + \frac{\tilde{p}_\perp^2}{2\tilde{z}^2} \frac{n \cdot \tilde{n}}{n \cdot p p \cdot \tilde{n}}, \quad (2.40)$$

and

$$k_\perp^\mu = \frac{\tilde{p}_\perp^2}{2\tilde{z}} \left(\frac{\tilde{n}^\mu}{\tilde{n} \cdot p} - \frac{n^\mu}{n \cdot p} \right) + \tilde{z}(1 - R)p^\mu + \tilde{k}_\perp^\mu. \quad (2.41)$$

Hence the leading scaling in the soft and collinear limits is the same in between the different parametrizations: the R factor is of $\mathcal{O}(1)$ in each of the soft and collinear limits, and the transverse momentum has the same leading scaling in both parametrizations, as well. The above result will also allow us to formulate local recoil schemes in which we choose a backward direction per collinear configuration, and to properly link this parametrization to our power counting rules.

2.5 Scaling of individual internal lines and vertices

In order to analyse how the individual diagrams scale in the relevant limits, we need to consider external lines carrying a hard momentum (which we refer to as ‘resolved’ in the sense of a strong ordering), internal lines with a hard momentum and a momentum

composed of soft, collinear or soft and collinear momenta. On top of this we consider ‘unresolved’ lines, which can become arbitrarily soft and/or collinear and for which both external as well as internal lines deliver the same scaling. It is clear that this distinction is only making sense if we separate the contributions in such a way that we need to consider collinear singular configurations only with respect to one line carrying a hard momentum, and soft contributions otherwise. Achieving such a separation will be discussed in Sec. 3.2, where we introduce one example of partitioning factors allowing for such a separation.

From the general form of the Sudakov decomposition Eq. (2.23) we then conclude that we need to assign scaling factors as outlined in Tables 1 and 2, respectively, where we refer to the different momentum flows as:

- h = external line with all momenta hard, possibly perturbed by a transverse momentum with respect to the hard direction, though we also consider the case in which the original direction is kept;
- $h+c$ = a sum of hard and collinear momenta;
- $h+s$ = a sum of hard and soft momenta; and
- $h+c+s$ = a sum of hard, collinear and soft momenta, for which, owing to the lower scaling power, it mostly is the soft limit which determines the properties.

For lines which are allowed to become arbitrarily unresolved, we refer to

- s = a sum of purely soft momenta, or a single soft momentum;
- c = a sum of purely collinear momenta, or a single collinear momentum; and
- $s+c$ = a combination of soft and collinear momenta.

Notice that the lines with the white square need to be considered as $\mathcal{O}(1)$ in any of the unresolved limits.

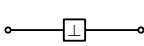



	h	$h+c$	$h+s$	$h+c+s$
	λ	λ	λ	λ
	1	λ	λ	λ
	λ^2	λ^2	λ	λ
	1	λ^2	λ	λ

Table 1: Power counting for hard line with (upper row in each entry) and without k_{\perp} recoil (lower row in each entry).

In Tab. 1, we show the scaling of hard lines (emitters or spectators) in all possible combinations of hard, soft and collinear momenta shown above. The first rows in each block

correspond to the case where the k_{\perp} recoil is included in the emitter mapping. The second rows correspond to the case without a k_{\perp} component which applies to spectator lines in general and can apply to emitters depending on the mapping used. Both of these mapping types are discussed in Sec. 4. The hard lines are signified by their horizontal orientation. In Tab. 2, vertical lines are used to refer to unresolved (soft or collinear) lines and the scaling is shown for the two different ‘box’ contributions. For both the hard and unresolved lines, the white box contributions do not have a scaling. Notice that we need to complete this picture by propagator factors which scale as $1/\lambda^2$ in the hard+collinear configuration, $1/\lambda$ in the hard+soft configuration as well as $1/\lambda$ in the hard+collinear+soft configuration. Completely unresolved propagators scale as $1/\lambda^2$ in a collinear or soft configuration, and as $1/\lambda$ in a soft+collinear configuration.



	s	c	s+c
	1	λ	λ
	1	λ^2	λ

Table 2: Power counting for unresolved lines.

3 Partitioning

An intrinsic assumption of our power counting is that we envisage to employ a partitioning of the soft behaviour into mutually exclusive collinear limits. This is important in order to organize a given observable into deviations from an ideal jet topology, but it will also give us a key to parametrize a kinematic mapping suited to collinear branching along a given direction and is thus of crucial importance to set up a parton shower algorithm. In this section we generalize both of the typically exploited partitionings to the multi-emission case. With the case of multiple emissions there are often multiple collinear combinations which can also be of different orders *i.e.* double or triple collinear. Whether a diagram contributes to a collinear limit or not is determined by the presence of internal propagators going on-shell in the respective limit. For k emissions, each diagram carries $2k$ internal propagators which can independently become singular in different collinear limits. It is the goal of our algorithm to partition these propagator factors into a set of splitting kernels, such that each kernel is only singular in the *one* collinear configuration it addresses. The partitioning factors themselves only contain soft singularities and for a given diagram add up to one across all collinear configurations. After partitioning, a specific momentum mapping can be applied to the amplitudes which contribute to a kernel, as the emitter and emission momenta can be labelled.

3.1 Basic purpose

The approach we use is best explained in a simple example of a rational function f singular in two independent variables x_1 and x_2 .

$$f(x_1, x_2) = \frac{n(x_1, x_2)}{S_1(x_1, x_2)S_2(x_1, x_2)}, \quad (3.1)$$

where $n(x_1, x_2)$ is a polynomial. We are firstly interested in the leading collinear singular behaviour for some specific configuration which corresponds to one of the $x_i \rightarrow 0$. Here, this is parametrized by $S_1 \rightarrow 0$ for $x_1 \rightarrow 0$ while $S_2 \neq 0$ and vice versa for $x_2 \rightarrow 0$. By defining the partitioning factors

$$\mathbb{P}_{(x_1)}^{(f)} = \frac{S_2}{S_1 + S_2}, \quad \mathbb{P}_{(x_2)}^{(f)} = \frac{S_1}{S_1 + S_2}, \quad (3.2)$$

we can decompose f into

$$f = \left[\mathbb{P}_{(x_1)}^{(f)} + \mathbb{P}_{(x_2)}^{(f)} \right] f = \frac{n(x_1, x_2)}{S_1(S_1 + S_2)} + \frac{n(x_1, x_2)}{S_2(S_1 + S_2)}. \quad (3.3)$$

This allows us to define the splitting kernels

$$\mathbb{U}_{(x_i)} = \mathbb{P}_{(x_i)}^{(f)} f = \frac{1}{S_i} \frac{n(x_1, x_2)}{S_1 + S_2}. \quad (3.4)$$

What we have achieved is a decomposition into objects which are singular solely in one of the variables. These objects will later be identified with so called splitting kernels. Moreover, the second factor on the right hand side of Eq. (3.4) is non-singular in any single $x_i \rightarrow 0$ collinear limit and therefore only contains soft singularities. Note that in this simple case, it is possible to set $x_i = 0$ in the numerator polynomial $n(x_1, x_2)$ without loss of information for the leading singular behaviour. Nevertheless, this is not possible in more complicated cases where the x_i can appear to some power > 1 in the denominator. Lastly, by only using the singular variables x_i in the partitioning, we make sure that we smoothly approach the original collinear singular behaviour of the function when both variables go to zero simultaneously. In the actual partitioning algorithm, this corresponds to keeping the correct soft-singular behaviour.

A second interesting option for partitioning is given by means of subtractions instead of partitioning factors of Eq. (3.3). It reads

$$f = \frac{1}{2} [f - \Delta_2 + \Delta_1] + (1 \leftrightarrow 2), \quad (3.5)$$

where

$$\Delta_1 = \frac{1}{S_1 S_2|_{x_1 \rightarrow 0}}, \quad \Delta_2 = \frac{1}{S_2 S_1|_{x_2 \rightarrow 0}}. \quad (3.6)$$

Here we use the fact that $S_1(x_2 \rightarrow 0)$ and $S_2(x_1 \rightarrow 0)$ are non-zero. In this case, a splitting kernel can be defined as

$$\mathbb{U}_{(x_1)} = \frac{1}{2} \left[\frac{1}{S_1 S_2} - \Delta_2 + \Delta_1 \right]. \quad (3.7)$$

This again gives a function which shows no singularity when $x_2 \rightarrow 0$, but reproduces the original singular behaviour when $x_1 \rightarrow 0$. We discuss this type of partitioning in Sec. 3.3.

3.2 Partial fractioning partitioning algorithm

As a first non-trivial example for our algorithm, we present the approach for the case of two emissions in this section. Firstly, it is expedient to define the various limits we are interested in. These can be represented by the set of collinear configurations \mathbf{C} for a given number of partons and emissions. In the two emission case, this set reads

$$\mathbf{C} = \{(i \parallel j \parallel k), (i \parallel j \parallel l), \dots, (i \parallel j)(k \parallel l), \dots\}, \quad (3.8)$$

where the notation $(i \parallel j)$ stands for two different external partons with momenta q_i and q_j becoming collinear. It consists of all configurations contributing to a triple collinear limit, *i.e.* all triplets and pairs-pairs one can build from the set of external partons. Next, we define the set $\mathbf{C}^{(d)}$ which contains only the configurations in which diagram d can become singular. As an example, we take the two emission interference diagram $A^{(1)}$ (see Fig. 3 in App. C), of which the propagator factors $\mathcal{P}(A_1)$ are given by

$$\mathcal{P}(A_1) = \frac{1}{S_{ij} S_{ijk} S_{kl} S_{jkl}}. \quad (3.9)$$

Here, we have used the notation

$$S_{ij} = S(q_i, q_j) \equiv (q_i + q_j)^2. \quad (3.10)$$

The singular collinear configurations and respective factors are collected in Table 3. Then, $\mathbf{C}^{(A_1)}$ is represented by the first column of the table. Then we can define \mathbf{S}_c^d , the set of

Configuration	Vanishing	Non-vanishing
$(i \parallel j \parallel k)$	$S_{ij} S_{ijk}$	$S_{kl} S_{jkl}$
$(i \parallel j \parallel l)$	S_{ij}	$S_{ijk} S_{kl} S_{jkl}$
$(i \parallel k \parallel l)$	S_{kl}	$S_{ij} S_{ijk} S_{jkl}$
$(j \parallel k \parallel l)$	$S_{kl} S_{jkl}$	$S_{ij} S_{ijk}$
$(i \parallel j), (k \parallel l)$	$S_{ij} S_{kl}$	$S_{ijk} S_{jkl}$

Table 3: Singular configurations and the relevant propagator factors for the two emission diagram A_1 .

vanishing S-invariants contained in diagram d for configuration c , which corresponds to the second column in Table 3. The partitioning factors for some singular configuration c and diagram d can then generally be defined as

$$\mathbb{P}_c^{(d)} \equiv \frac{F_c^{(d)}}{\mathbb{F}^{(d)}}, \quad (3.11)$$

where the cancelling factors $F_c^{(d)}$ are given by

$$F_c^{(d)} = \left(\prod_{S_{c'} \in \mathbf{S}_c^{(d)}} S_{c'} \mathcal{P}(\mathcal{A}^{(d)}) \right)^{-1} \zeta^p, \quad (3.12)$$

and

$$\mathbb{F}^{(d)} \equiv \sum_{c \in \mathbf{C}^{(d)}} F_c^{(d)}. \quad (3.13)$$

The cancelling factors $F_c^{(d)}$ correspond to the last column in Table 3. Lastly, we have introduced the scale ς^p in order to keep the partitioning factors dimensionless. The power p needs to be chosen such that all cancelling factors carry the same mass dimension.²

In the following, we assume that i and l are hard partons. For topology $A^{(1)}$, this provokes that we only need to deal with the three leading singular configurations of Table 3. Its cancelling factors are

$$F_{(ijk)}^{(A^{(1)})} = \left(S_{ij} S_{ijk} A^{(1)} \right)^{-1} = S_{kl} S_{jkl}, \quad (3.14a)$$

$$F_{(jkl)}^{(A^{(1)})} = \left(S_{kl} S_{jkl} A^{(1)} \right)^{-1} = S_{ij} S_{ijk}, \quad (3.14b)$$

$$F_{(ij)(kl)}^{(A^{(1)})} = \left(S_{ij} S_{kl} A^{(1)} \right)^{-1} = S_{ijk} S_{jkl}, \quad (3.14c)$$

which corresponds to the entries of the third column of Table 3. Then, the amplitude's fully partitioned propagator is given by

$$\sum_{c \in \mathbf{C}_{A^{(1)}}} \mathbb{P}_c^{(A^{(1)})} \mathcal{P}(A^{(1)}) = \frac{1}{S_{kl} S_{jkl} + S_{ij} S_{ijk} + S_{ijk} S_{jkl}} \times \left(\frac{1}{S_{ij} S_{ijk}} + \frac{1}{S_{kl} S_{jkl}} + \frac{1}{S_{ij} S_{kl}} \right). \quad (3.15)$$

The first, second and third term will give leading singular contributions to splitting kernels $\mathbb{U}_{(ijk)}$, $\mathbb{U}_{(jkl)}$ and $\mathbb{U}_{(ij)(kl)}$, respectively.

Note that topologies with only one hard line, *i.e.* the self-energy like ones need no partitioning due to the absence of a recoiler that the emissions could become collinear to.

In Tab. 4, we show the collinear and soft scalings for the two-emission topologies of App. C together with their fractional partitioning factors for the $(i \parallel j \parallel k)$ configuration. Eventually, these scalings need to be combined with the respective numerators scalings discussed in Sec. 2.5 in order to determine which topology contributes to a splitting kernel at a given power in λ . We show the resulting table in Sec. 6.

The partitioning factors as defined in Eq. (3.11) fulfil two important requirements as already mentioned in Sec. 3.1., *viz.*

1. Non-singular behaviour in any collinear limit,
2. Soft-collinear and purely soft limits are reproduced correctly.

The first property is guaranteed by the fact that the sum in Eq. (3.13) does not vanish in *any* collinear limit. One can show this fact by realising that for all given collinear configurations

²Note that this scale could be avoided by only partitioning into the *leading* singular behaviours. The caveat is that there are diagrams for which it is *a priori* unclear which of the singular structures will give leading contributions to some kernel. Therefore, it is safer in this sense to simply partition into all possible singular structures.

	CC	CS	SC	SS
$A^{(1)}$	$1/\lambda^4$	$1/\lambda^4$	$1/\lambda^2$	$1/\lambda^4$
$A^{(2)}$	$1/\lambda^4$	$1/\lambda^3$	$1/\lambda^3$	$1/\lambda^4$
$A^{(3)}$	$1/\lambda^4$	$1/\lambda^3$	$1/\lambda^2$	$1/\lambda^4$
$A^{(4)}$	$1/\lambda^6$	$1/\lambda^4$	$1/\lambda^3$	$1/\lambda^5$
$A^{(5)}$	$1/\lambda^6$	$1/\lambda^3$	$1/\lambda^3$	$1/\lambda^6$
$B^{(1)}$	$1/\lambda^6$	$1/\lambda^6$	$1/\lambda^3$	$1/\lambda^4$
$B^{(2)}$	$1/\lambda^6$	$1/\lambda^4$	$1/\lambda^5$	$1/\lambda^4$
$B^{(3)}$	$1/\lambda^6$	$1/\lambda^5$	$1/\lambda^3$	$1/\lambda^5$
$B^{(4)}$	$1/\lambda^6$	$1/\lambda^6$	$1/\lambda^3$	$1/\lambda^4$
$B^{(5)}$	$1/\lambda^6$	$1/\lambda^4$	$1/\lambda^5$	$1/\lambda^4$
$B^{(6)}$	$1/\lambda^6$	$1/\lambda^5$	$1/\lambda^3$	$1/\lambda^5$
$X^{(1)}$	$1/\lambda^4$	$1/\lambda^4$	$1/\lambda^4$	$1/\lambda^4$
$X^{(2)}$	$1/\lambda^4$	$1/\lambda^4$	$1/\lambda^2$	$1/\lambda^2$
$E^{(1)}$	$1/\lambda^8$	$1/\lambda^6$	$1/\lambda^4$	$1/\lambda^4$
$E^{(2)}$	$1/\lambda^8$	$1/\lambda^5$	$1/\lambda^5$	$1/\lambda^4$
$E^{(3)}$	$1/\lambda^8$	$1/\lambda^5$	$1/\lambda^4$	$1/\lambda^5$
$E^{(4)}$	$1/\lambda^8$	$1/\lambda^5$	$1/\lambda^4$	$1/\lambda^5$
$E^{(5)}$	$1/\lambda^8$	$1/\lambda^4$	$1/\lambda^4$	$1/\lambda^6$

Table 4: Scaling for propagator times partitioning factor of two emission single emitter topologies when partitioned to $(i \parallel j \parallel k)$. Here, ‘CC’ refers to the triple collinear limit where $i \parallel j \parallel k$, ‘CS’ refers to $(i \parallel j)$ with soft k , ‘SC’ to $(i \parallel k)$ and j soft and ‘SS’ is the double soft limit where both j and k are soft.

$c \in \mathbf{C}^{(d)}$, the partitioning factors $F_c^{(d)} \neq 0$ per definition. An example is $c = (i \parallel j)(k \parallel l)$ for which $F_{c_1}^{(A^{(1)})} = \varsigma S_{ijk} S_{jkl} \neq 0$ in said configuration. It can be that $F_c^{(d)}$ vanishes in another configuration c' , but not all of them simultaneously. The reason is that in the case where partitioning is carried out, there are necessarily recoiler partons present leading to the fact that not all propagator factors of the respective diagram vanish simultaneously. In all other configurations $c \notin \mathbf{C}^{(d)}$, we know that $(A^{(d)})^{-1} \neq 0$ and therefore, neither the partitioning factors $F_c^{(A_d)}$ can vanish here. Thus, there is no configuration where all $F_c^{(A_d)} = 0$ simultaneously for a given diagram d .

Secondly, the property of the correct scaling behaviour in soft- and soft-collinear limits is guaranteed by the fact that for a given diagram, we only use the S -invariants appearing in the respective diagram to construct the partitioning factors, which form a partition of unity. Therefore, there is no spurious finite remainder in $\mathbb{F}^{(d)}$ that could spoil the approach of the original soft singularity.

We stress that the analysis in this section has focused on the case that we have identified certain partons as those carrying the hard momentum. Additional combinatorics are thus needed if several partons in the same jet could carry the hard momentum, but

in an algorithmic implementation, see Sec. 6, we will be able to decide at each branching which of the daughter particles is to carry the hard momentum, and whether that particular configuration will then contribute to the leading behaviour, *e.g.* our power counting directly implies that a hard quark transitioning into a soft quark and a hard gluon will be immediately suppressed by the $\sqrt{z_i z_j}$ factor we associate to the effective quark-gluon vertex.

3.3 Subtraction (angular ordered) partitioning algorithm

An alternative approach to partitioning is to isolate and subtract collinear divergencies in a way that a single collinear divergence remains in the diagram just considered. For one emission, this procedure leads to angular ordering, essentially using

$$\frac{1}{S_{ij} S_{jk}} = \frac{1}{S_{ik}} \frac{1}{2E_j^2} \left(\frac{n_i \cdot n_k}{n_i \cdot n_j n_j \cdot n_k} - \frac{1}{n_j \cdot n_k} + \frac{1}{n_i \cdot n_j} \right) + (i \leftrightarrow k), \quad (3.16)$$

where we have decomposed the momenta into energies and directions, $p_j = E_j n_j$; in this case, any measure of energy could have been used, *i.e.* in general we consider $E_i = T \cdot p_i$ with some timelike vector T . In the above expression, the first term is singular only in the $(i||j)$ configuration, while the second one is singular in the complementary $(k||j)$ limit. In this section we show how this paradigm can be generalized to a larger number of emissions and we find that the resulting partitioning shows the same scaling behaviour as the partial fractioning variant, thus allowing to use the same power counting.

The basic idea of the subtraction partitioning now starts from a slight re-write of the angular ordering logic; to this extent rewrite Eq. (3.16) as

$$\frac{1}{S_{ij} S_{jk}} = \frac{1}{2} \left(\frac{1}{S_{ij} S_{jk}} - \frac{E_k}{E_j} \frac{1}{S_{ik} S_{jk}} + \frac{E_i}{E_j} \frac{1}{S_{ik} S_{ij}} \right) + (i \leftrightarrow k). \quad (3.17)$$

The second term in the parentheses has been constructed to subtract off the $1/S_{jk}$ divergence upon replacing $1/S_{ij}$ by its limiting expression for $(j||k)$, *i.e.*

$$S_{ij} \xrightarrow{(j||k)} E_i E_j n_i \cdot n_k = \frac{E_j}{E_k} S_{ik} \quad (3.18)$$

and the second term adds back what has been subtracted in the term with i and k interchanged. This decomposition allows to define the partitioned propagator

$$\mathbb{P}_{(i||j)} \left[\frac{1}{S_{ij} S_{jk}} \right] = \frac{1}{2} \left(\frac{1}{S_{ij} S_{jk}} - \Delta_{(j||k)} + \Delta_{(i||j)} \right), \quad (3.19)$$

with

$$\Delta_{(i||j)} = \frac{E_i}{E_j} \frac{1}{S_{ik} S_{ij}}, \quad \Delta_{(j||k)} = \frac{E_k}{E_j} \frac{1}{S_{ik} S_{jk}}. \quad (3.20)$$

It fulfils the expectation of giving back the original singular scaling behaviour in the $(i || j)$ case while being non-singular when $(j || k)$.

In fact, this construction is algorithmic and can be generalized to more than one emission; the only complication which arises is in the fact that several collinear limits

might be overlapping, *i.e.* some of the Δ factors themselves contain sub-singularities, and in turn these need to be subtracted out of the possible subtraction terms to guarantee that one resulting partition summand truly only reflects one collinearly singular configuration.

In particular we can write the procedure to construct subtraction terms as

$$\Delta_{\tau_1; \tau_2, \dots, \tau_m}[P] = \mathbb{F}_{\tau_1}[P] \left(\mathbb{S}_{\tau_1}[P] - \overline{\sum_{\mathcal{S}/\tau_1} \Delta_{\tau_{i_1}; \tau_{i_2}, \dots, \tau_{i_{m-1}}} [\mathbb{S}_{\tau_1}[P]]} \right), \quad (3.21)$$

where $\mathbb{F}_{\tau_1}[P]$ indicates to collect those factors from the propagator factor P which are non-singular in the limit identified by τ_1 and to replace them by their limiting expressions in this limit. Conversely, $\mathbb{S}_{\tau_1}[P]$ indicates to take the singular factors. Moreover, \mathcal{S} is the set of singular configurations of $\mathbb{S}_{\tau_1}[P]$ and the summation symbol stands for dividing by the number of terms of the sum. The indices after the semicolon in Δ signify the order of the limits taken beforehand which can play a role if these limits do not commute in terms of the partitioning Δ 's. We then proceed to subtract the remaining overlapping singular limits, and we define

$$\Delta_{\tau_1; \tau_2, \dots, \tau_m}[P] = \Delta_{\tau_2; \tau_3, \dots, \tau_m}[P] \quad \text{if } P \text{ not } \tau_1 \text{ collinear singular}, \quad (3.22)$$

$\Delta_{\sigma;}(P) = 0$ if P is non-singular in σ , and $\Delta_{\sigma;}(P) = \mathbb{F}_{\sigma}[P]\mathbb{S}_{\sigma}[P]$ otherwise. The resulting partitioned propagator then is

$$\mathbb{P}_{\sigma}[P] = \frac{1}{m} \left(P + (m-1)\Delta_{\sigma; \tau_1, \dots, \tau_{m-1}}[P] - \sum_{i=1}^{m-1} \Delta_{\tau_i; \tau_1, \dots, \tau_{i-1}, \sigma, \tau_{i+1}, \dots, \tau_{m-1}}[P] \right), \quad (3.23)$$

where $\sigma, \tau_1, \dots, \tau_{m-1}$ denote the m configurations in which P can develop collinear singularities.

As an example, we show this version of the partitioning algorithm again for the amplitude $A^{(1)}$ with propagators factors of Eq. (3.9). The configurations where $\mathcal{P}(A^{(1)})$ has a leading singularity are

$$\begin{aligned} \tau_1 &= (i \parallel j \parallel k), \\ \tau_2 &= (j \parallel k \parallel l), \\ \tau_3 &= (i \parallel j)(k \parallel l). \end{aligned} \quad (3.24)$$

Therefore, $m = 3$ in this case. First, we collect the limiting expressions in these configurations, *i.e.*

$$\begin{aligned} \mathbb{F}_{\tau_1}[\mathcal{P}(A^{(1)})] &= \frac{1}{S_{kl}S_{jkl}} \Big|_{\tau_1} = \frac{E_i^2}{E_k(E_j + E_k)} \frac{1}{S_{il}^2}, \\ \mathbb{F}_{\tau_2}[\mathcal{P}(A^{(1)})] &= \frac{1}{S_{ij}S_{ijk}} \Big|_{\tau_2} = \frac{E_l^2}{E_j(E_j + E_k)} \frac{1}{S_{il}^2}, \\ \mathbb{F}_{\tau_3}[\mathcal{P}(A^{(1)})] &= \frac{1}{S_{ijk}S_{jkl}} \Big|_{\tau_3} = \frac{E_i^2 E_l^2}{E_k(E_i + E_j) E_j(E_k + E_l)} \frac{1}{S_{il}^2}. \end{aligned} \quad (3.25)$$

Note that a single index specification is sufficient here, because the order of taking the limits does not matter in this example. Then, we can construct the first subtraction term, *viz.*

$$\Delta_{\tau_1}[\mathcal{P}(A^{(1)})] = \mathbb{F}_{\tau_1}[\mathcal{P}(A^{(1)})] \sum_{\tau \in \mathbf{S}/\tau_1} \left(\frac{1}{S_{ij}S_{ijk}} - \Delta_{\tau} \left[\frac{1}{S_{ij}S_{ijk}} \right] \right). \quad (3.26)$$

This term is supposed to only cancel $(i \parallel j \parallel k)$ -singularities. Therefore, we subtract off the overlapping sub-singularity in the parentheses via

$$\Delta_{\tau_3} \left[\frac{1}{S_{ij}S_{ijk}} \right] = \mathbb{F}_{\tau_3} \left[\frac{1}{S_{ijk}} \right] \frac{1}{S_{ij}}, \quad (3.27)$$

where τ_3 is the only relevant configuration in the sum of Eq. (3.26), because this sub-propagator is non-singular in τ_2 . The same procedure applies to the other two subtraction terms. Eventually, we find

$$\begin{aligned} \Delta_{\tau_1}[\mathcal{P}(A^{(1)})] &= \frac{E_i^2}{E_k(E_j + E_k)} \frac{1}{S_{il}^2} \left(\frac{1}{S_{ij}S_{ijk}} - \frac{E_i E_l}{E_k(E_i + E_j)} \frac{1}{S_{il}S_{ij}} \right), \\ \Delta_{\tau_2}[\mathcal{P}(A^{(1)})] &= \frac{E_l^2}{E_j(E_j + E_k)} \frac{1}{S_{il}^2} \left(\frac{1}{S_{kl}S_{jkl}} - \frac{E_i E_l}{E_j(E_k + E_l)} \frac{1}{S_{il}S_{kl}} \right), \\ \Delta_{\tau_3}[\mathcal{P}(A^{(1)})] &= \frac{E_i^2 E_l^2}{E_k(E_i + E_j) E_j(E_k + E_l)} \frac{1}{S_{il}^2} \left(\frac{1}{S_{ij}S_{kl}} - \frac{E_i}{E_k} \frac{1}{S_{il}S_{ij}} - \frac{E_l}{E_j} \frac{1}{S_{il}S_{kl}} \right). \end{aligned} \quad (3.28)$$

Then, using Eq. (3.23), the partitioned propagator of $A^{(1)}$ is given by

$$\begin{aligned} \mathcal{P}(A^{(1)}) &= \frac{1}{3} \left(\frac{1}{S_{ij}S_{ijk}S_{kl}S_{jkl}} + 2\Delta_{\tau_1}[\mathcal{P}(A^{(1)})] - \Delta_{\tau_2}[\mathcal{P}(A^{(1)})] - \Delta_{\tau_3}[\mathcal{P}(A^{(1)})] \right), \\ &+ \frac{1}{3} \left(\frac{1}{S_{ij}S_{ijk}S_{kl}S_{jkl}} - \Delta_{\tau_1}[\mathcal{P}(A^{(1)})] + 2\Delta_{\tau_2}[\mathcal{P}(A^{(1)})] - \Delta_{\tau_3}[\mathcal{P}(A^{(1)})] \right), \\ &+ \frac{1}{3} \left(\frac{1}{S_{ij}S_{ijk}S_{kl}S_{jkl}} - \Delta_{\tau_1}[\mathcal{P}(A^{(1)})] - \Delta_{\tau_2}[\mathcal{P}(A^{(1)})] + 2\Delta_{\tau_3}[\mathcal{P}(A^{(1)})] \right), \end{aligned} \quad (3.29)$$

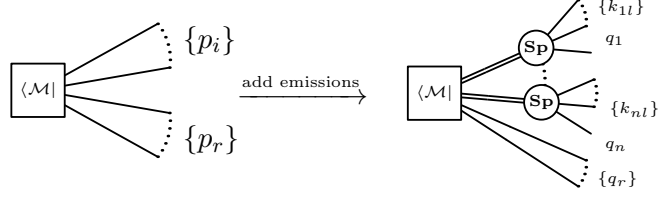
where the first, second and third line are $\mathbb{P}_{\tau_1}[\mathcal{P}(A^{(1)})]$, $\mathbb{P}_{\tau_2}[\mathcal{P}(A^{(1)})]$ and $\mathbb{P}_{\tau_3}[\mathcal{P}(A^{(1)})]$, respectively.

4 Momentum mapping

In this section, we define two instances of a momentum mapping in terms of the Sudakov-like decomposition of Eq. (2.22) where momentum conservation between emitters and emissions is manifest and a global Lorentz-transformation is introduced for momentum conservation when emissions are added to a given process, as already advertised in Sec. 2.3. Using the dictionary of Sec. 2.4, both versions of the mapping are compatible with the power counting rules introduced in Sec. 2.5.

The momentum mapping is set up in a language inspired by parton showers. In a parton shower setup, one starts from a set of massless on-shell momenta of a hard

process which are then dressed up with emissions, which again are massless and on-shell. Diagrammatically, this can be represented by



where the p_i are the momenta to which emissions are added with $i \in \mathbf{S}$ (“splitters”) and the p_r are available for recoil absorption with $r \in \mathbf{R}$ (“recoilers”). This leads us to define the momenta after emissions in terms of the forward (p_i), backward (n_i) and transverse components ($n_{\perp,l}^{(i)}$) as

$$q_r \equiv \frac{1}{\hat{\alpha}} \Lambda p_r , \quad (4.1a)$$

$$\bar{q}_i \equiv \frac{1}{\hat{\alpha}} \Lambda [(1 - A_i) p_i] \quad (\text{unbalanced}) , \quad (4.1b)$$

$$q_i \equiv \frac{1}{\hat{\alpha}} \Lambda [(1 - A_i) p_i + (y_i - \tilde{B}_i) n_i - \tilde{n}_{\perp}^{(i)}] \quad (\text{balanced}) , \quad (4.1c)$$

$$k_{il} \equiv \frac{1}{\hat{\alpha}} \Lambda \left[\alpha_{il} p_i + \tilde{\beta}_{il} n_i + \sqrt{\alpha_{il} \tilde{\beta}_{il}} n_{\perp,l}^{(i)} \right] , \quad (4.1d)$$

where we show one version with balanced (q_i) and one with unbalanced (\bar{q}_i) transverse components and use the shorthands

$$A_i \equiv \sum_{l \in \mathbf{E}_i} \alpha_{il} , \quad \tilde{B}_i \equiv \sum_{l \in \mathbf{E}_i} \tilde{\beta}_{il} , \quad \tilde{\beta}_{il} = (1 - A_i) \beta_{il} , \quad \tilde{n}_{\perp}^{(i)} \equiv \sum_{l \in \mathbf{E}_i} \sqrt{\alpha_{il} \tilde{\beta}_{il}} n_{\perp,l}^{(i)} , \quad (4.2)$$

Note the inclusion of a Lorentz transformation Λ together with a scaling $\hat{\alpha}$ which are needed for the non-trivial global recoil and momentum conservation. The latter leads to

$$\sum_{i \in \mathbf{S}} \left(q_i + \sum_{l \in \mathbf{E}_i} k_{il} \right) + \sum_{r \in \mathbf{R}} q_r = Q , \quad (4.3)$$

where Q is the original overall momentum transfer

$$Q \equiv \sum_{i \in \mathbf{S}} p_i + \sum_{r \in \mathbf{R}} p_r . \quad (4.4)$$

Inserting Eq. (4.1) into Eq. (4.3) gives

$$Q = \frac{1}{\hat{\alpha}} \Lambda \left[\sum_{r \in \mathbf{R}} p_r + \left(\sum_{i \in \mathbf{S}} p_i + y_i n_i \right) \right] . \quad (4.5)$$

Squaring this equation fixes the scaling to

$$\hat{\alpha}^2 = \frac{(Q + N)^2}{Q^2} , \quad (4.6)$$

where

$$N \equiv \sum_{i \in \mathbf{S}} y_i n_i . \quad (4.7)$$

Using Lorentz-invariance of amplitudes, $\hat{\alpha}$ provides the means to implement a global recoil as shown in Eq. (2.20).

The numbers α_{il} and β_{il} take values in $(0, 1)$ and parametrize the soft and collinear behaviour of the emission momenta k_{il} , as well as the emitter momenta q_i . In the balanced version of the mapping, y_i quantifies the off-shellness of the emitter-emission system. This can be seen by squaring the momentum sum for emissions and the emitter, *i.e.*

$$\left(q_i + \sum_l k_{il} \right)^2 = y_i 2p_i \cdot n_i . \quad (4.8)$$

Therefore, both the soft and collinear limits are parametrized by the $y_i \rightarrow 0$ limit. The y_i are fixed via the on-shell relations for the q_i , *i.e.*

$$y_i = (1 - A_i) B_i - \frac{(\tilde{n}_\perp^{(i)})^2}{2p_i \cdot n_i (1 - A_i)} , \quad (4.9)$$

which shows that a scaling in y_i is fixed by scaling the α_{il} and β_{il} . Instead, for the unbalanced version of the mapping, we formally have $y_i = \tilde{B}_i$ and $\tilde{n}_\perp^{(i)} = 0$ and overall momentum transfer is given by

$$\left(\bar{q}_i + \sum_l k_{il} \right)^2 = \tilde{B}_i 2p_i \cdot n_i + (\tilde{n}_\perp^{(i)})^2 . \quad (4.10)$$

The on-shellness of the emission momenta k_{il} fixes the virtuality of the transverse components as

$$\left(n_{\perp,l}^{(i)} \right)^2 = -2p_i \cdot n_i . \quad (4.11)$$

These components are further determined by the transversality relations

$$p_i \cdot n_{\perp,l}^{(i)} = 0 \quad \text{and} \quad n_i \cdot n_{\perp,l}^{(i)} = 0, \quad \forall i \in \mathbf{S} \text{ and } \forall l \in \mathbf{E}_i . \quad (4.12)$$

We can choose n_i locally w.r.t. jet directions while simultaneously using the gauge vector n to expand in a global basis of spinors and polarization vectors. The effect of such a choice is discussed at the end of Sec. 2.3. A suitable choice for the (in principle arbitrary) lightlike backwards components n_i is

$$n_i^\mu = Q^\mu - \frac{Q^2}{2p_i \cdot Q} p_i^\mu . \quad (4.13)$$

In App. A, we discuss the phase space factorisation in terms using this type of momentum mapping.

The momentum mapping allows us to parametrise the scaling of the momentum components in the style of SCET [29] according to the following table

k_{il}	$(p_i, n_i, n_{\perp,l}^{(i)})$	$(\alpha_{il}, y_i, \beta_{il})$
(forward) collinear	$Q(1, \lambda^2, \lambda)$	$(1, \lambda^2, \lambda^2)$
soft	$Q(\lambda, \lambda, \lambda)$	$(\lambda, \lambda, \lambda)$.

The overall scaling in λ can subsequently be used to study the IR singular behaviour of an emission amplitude. For this purpose, we present all relevant dot-products which can appear in squared emission amplitudes in terms of the momentum mapping of Eq. (4.1), *viz.*

$$S(q_i, K_i) = y_i 2p_i \cdot n_i, \quad (4.14a)$$

$$S(q_i, k_{il}) = \frac{2}{\hat{\alpha}^2} \left[\left(\alpha_{il}(y_i - \tilde{B}_i) + \tilde{\beta}_{il}(1 - A_i) \right) p_i \cdot n_i - \sqrt{(1 - A_i)\alpha_{il}\tilde{\beta}_{il}} n_{\perp,l}^{(i)} \cdot \tilde{n}_{\perp}^{(i)} \right], \quad (4.14b)$$

$$S(k_{il}, k_{il'}) = \frac{2}{\hat{\alpha}^2} \left[(\alpha_{il}\tilde{\beta}_{il'} + \alpha_{il'}\tilde{\beta}_{il}) p_i \cdot n_i + \sqrt{\alpha_{il}\tilde{\beta}_{il}\alpha_{il'}\tilde{\beta}_{il'}} n_{\perp,l}^{(i)} \cdot n_{\perp,l'}^{(i)} \right], \quad (4.14c)$$

$$S(k_{il}, q_r) = \frac{2}{\hat{\alpha}^2} \left[\alpha_{il} p_i \cdot p_r + \tilde{\beta}_{il} n_i \cdot p_r + \sqrt{\alpha_{il}\tilde{\beta}_{il}} n_{\perp,l}^{(i)} \cdot p_r \right], \quad (4.14d)$$

$$S(q_i, q_r) = \frac{2}{\hat{\alpha}^2} \left[(1 - A_i) p_i \cdot p_r + (y_i - \tilde{B}_i) n_i \cdot p_r - \sqrt{1 - A_i} \tilde{n}_{\perp}^{(i)} \cdot p_r \right], \quad (4.14e)$$

where we have used the shorthand

$$K_i \equiv \sum_{l \in \mathbf{E}_i} k_{il}. \quad (4.15)$$

In the unbalanced version of the mapping, the following S -invariants change:

$$S(\bar{q}_i, K_i) = \tilde{B}_i 2p_i \cdot n_i + (\tilde{n}_{\perp}^{(i)})^2, \quad (4.16a)$$

$$S(\bar{q}_i, k_{il}) = \frac{2p_i \cdot n_i}{\hat{\alpha}^2} (1 - A_i) \tilde{\beta}_{il}, \quad (4.16b)$$

$$S(\bar{q}_i, q_r) = \frac{2}{\hat{\alpha}^2} [(1 - A_i) p_i \cdot p_r], \quad (4.16c)$$

The λ -scaling of these invariants for both variants of the mapping can be summarized as

k_{il}	$S(q_i, K_i)$	$S(q_i, k_{il})$	$S(k_{il}, k_{il'})$	$S(k_{il}, q_r)$	$S(q_i, q_r)$
collinear	λ^2	λ^2	λ^2	1	1
soft	λ	λ	λ^2	λ	1

This information is helpful in determining the set of diagrams that contributes to a given soft, collinear or mixed limit and it is, of course, compatible with the scaling we have used in deriving our effective Feynman rules.

5 Splitting kernels

In this section, we will discuss how we can built up full *splitting kernels* in combination of our findings on the power counting, the partitioning and the underlying momentum mapping. Using the partitioning factors of Sec. 3.2, they can be defined as follows:

$$\mathbb{U}_c \equiv \sum_d \left[\mathbb{P}_c^{(d)} \mathcal{A}^{(d)} \right]. \quad (5.1)$$

$\mathcal{A}^{(d)}$ represents a certain topology under consideration, *i.e.* a configuration with a fixed set of propagators in the amplitude and the conjugate amplitude. We find it convenient to represent these still as cut diagrams, however it should be clear that their meaning is to be taken in the sense of the density operator as discussed in Sec. 2.

We choose the latter language with the intent of making an iterative procedure in treating emissions more tangible. The subscript c stands for the collinear configuration that the kernel is addressing. An example is the triple-collinear configuration $c = (i \parallel j \parallel k)$ for the two emission case, where $\mathbb{U}_{(ijk)}$ contains all leading singular contributions for the momenta q_i , q_j and q_k becoming collinear. The fact that $\mathbb{U}_{(ijk)}$ contains no other leading singular structures is assured via the partitioning factors $\mathbb{P}_{ijk}^{(d)}$. Schematically, Eq. (5.1) can be paraphrased as

$$\begin{aligned}
 \mathbb{U}_c = & \text{Diagram 1} + \mathbb{P}_c^{(d_M)} \times \text{Diagram 2} + \\
 & \mathbb{P}_c^{(d_I)} \times \text{Diagram 3} \tag{5.2}
 \end{aligned}$$

In the language of cut diagrams, the first term can be read as *self-energy like* contributions, *i.e.* contributions where the partons on the amplitude and conjugate amplitude side originate from the same splitter parton. In lightcone gauge, these contributions contain the leading collinear singularities. The second term in Eq. (5.2) refers to contributions where partons on the amplitude side identified with partons from several different splitting groups on the conjugate side. These will be relevant for *mixed* soft-collinear limits. Lastly, the third term stands for diagrams where none of the splitter partons on the conjugate side are identified with the splitter on the amplitude side. They correspond to *interference* diagrams which in lightcone gauge are relevant for soft limits only.

In addition to the contributions depicted in Eq. (5.2), one can have multiple emitters on the amplitude side. For two emissions, this corresponds to configurations contributing to double-unresolved limits such as $c' = (i \parallel j)(k \parallel l)$ where two sets of partons exhibit independent collinearities. The construction of the respective splitting kernels follow the same logic as for the single emitter case, the main difference being that one can not categorize the various contributions into self-energy like, mixed and interference diagrams as easily.

As a next step, we can insert the momentum mapping of Sec. 4 for a given configuration c into the amplitudes entering the splitting kernel \mathbb{U}_c . This step essentially fixes the notion of which partons are considered as emitters, recoilers and emissions. Having made sure that there are no other singular configurations that need addressing here, we can be certain

that all leading singular contributions can be captured via the insertion of the respective momentum mapping.

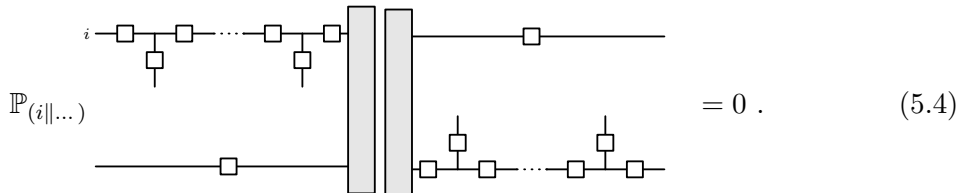
5.1 Power counting algorithm

In order to provide a general rule for which contributions to keep in terms of our power counting in splitting kernels, several remarks are in order. First of all, it is easy to show the fact that interference contributions do not contribute to leading collinear limits using our formalism. The most important rule to make use of here is the fact that amplitudes which only contain forward components of the same collinear sector vanish exactly (this was already mentioned at the end of Sec. 2.1), *i.e.*



$$= 0, \quad (5.3)$$

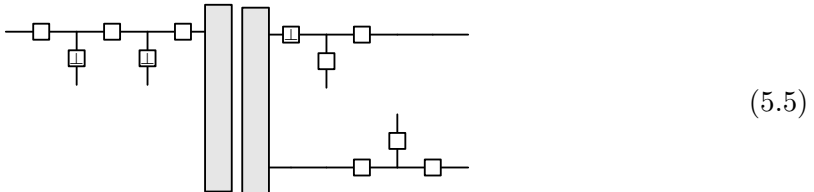
Now, in order for a diagram to contribute in the leading collinear limit, it must have a scaling of $1/\lambda^{2k}$, where k is the number of emissions. In interference contributions, only the propagator factors of the splitter side give a collinear scaling as long as we use either version of our partitioning algorithm to get rid of collinearities on the interferer legs. Then, the propagator factors of the diagram shown in Eq. (5.4) give a scaling of $1/\lambda^{2k}$. This means that such contributions can only give rise to leading collinearities when the numerator does not scale, meaning that one would need only the forward components of each line, or white boxes respectively. Knowing that the respective vertices exactly vanish on the splitter side, we find



$$= 0. \quad (5.4)$$

The above holds generically also for appearances of the collinear three-gluon vertex of Eq. (2.31b). This shows that interferences do not contribute to the leading collinear limits.

For contributions that are relevant for mixed soft-collinear behaviour, a general discussion is more involved. We start here by discussing of two emissions, but expect this pattern to hold also for $k > 2$. The leading singular amplitudes will have at least two (\perp)-boxes on the splitter and one on the conjugate side. An example is



$$(5.5)$$

The numerator of these leading amplitudes goes as λ_c^3 while the denominator goes as λ_c^6 in the purely collinear limit. Therefore, soft-collinear mixed contributions do not contribute leadingly here.

clarity, *i.e.*

$$(5.8)$$

Here, we denote hard partons providing different forward directions by h_1 and h_2 . The existence of these hard partons can be guaranteed via the respective choice of an observable, such as a two-jet observable in this example. In other words, phase space configurations where the latter would become soft or collinear are cut off by the observable. All other partons in the process, *i.e.* the *emissions*, can become soft or collinear w.r.t. the hard ones. Now, the partitioning factor $\mathbb{P}_{c||h_1}^{(d)}$ works such that only configurations with collinearities to parton h_1 give rise to a leading singular behaviour of the kernel. Therefore, parton h_2 can be treated without loss of generality as a *recoiler* which will only be of importance for soft limits. Let us denote the set of partons on the amplitude side by I , the the ones connected to h_1 on the conjugate side by \bar{I} and the ones connected to h_2 by \bar{J} . The observable guarantees that I contains a hard parton.

We can use the projector rules of Eq. (2.30) to establish factorisation in the following sense:

$$(5.9)$$

For the splitter line on the amplitude side, there are no (\perp)-components coming from the hard amplitude when transverse momenta are balanced between the emitter and emissions. Then, the leading contribution from this side comes just from the forward momentum component.³ The leading contributions on recoiler lines come from its forward components which are from different collinear sectors and therefore, Eq. (5.3) does not apply here. The situation is more complicated for the conjugate side splitter line. Here, the (\perp)-components entering the hard amplitude are in general unbalanced and could give contributions to the leading singular limits. Nevertheless, we suspect that only the combination shown in Eq. (5.9) could give such a contribution. Then, by including the projection operators in the splitting amplitude, one can neglect all but the forward momenta components from the hard amplitude.

The reason for our suspicion comes from the one and two emission examples. For one emission, there are no (\perp)-components coming from the hard amplitude at all by choice of a respective recoil scheme. For two emissions, there are contributions from such components, but we can use Eq. (2.30) to decompose them, *i.e.*

$$(5.10)$$

³Note that a few of the two emission amplitudes have a black box appearing on the hard amplitude line. Nevertheless, Tab. 6 shows that these could only contribute to the leading soft-collinear limits. Moreover, one has to check whether such contributions vanish identically on a case by case basis.

	C	S		C	S
	λ	λ		λ	λ
	λ	1		λ^2	λ^2
	λ	λ		λ^2	λ^2
	λ^2	λ		λ^2	λ
	λ^2	λ^2			
	λ^2	λ			
	1	1			
	λ	1			

Table 5: Single emission subamplitudes up to $\mathcal{O}(\lambda^2)$ collinear (C) or soft (S) scaling for both longitudinal and transverse vertices. Emission lines going upwards (downwards) signify interferer (splitter) subamplitudes.

$$\begin{aligned}
\mathbb{U}_{(ij)} = \mathbb{P}_{(ij)} & \left(\begin{array}{c} \text{Diagram 1} \\ \text{Diagram 2} \end{array} + \begin{array}{c} \text{Diagram 3} \\ \text{Diagram 4} \end{array} \right) \quad (5.12) \\
& + \begin{array}{c} \text{Diagram 5} \\ \text{Diagram 6} \end{array} \\
& + \begin{array}{c} \text{Diagram 7} \\ \text{Diagram 8} \end{array}
\end{aligned}$$

We now want to exhibit the interplay between soft and collinear contributions in this

different kernels for collinear sectors. Especially in view of the more complicated colour structures pertaining to the interference diagrams, our formalism might be beneficial as it explicitly appreciates the fact that the colour correlations are collinear finite.

Our partitioning algorithms allow us, however, to apply a similar logic to the interplay of soft and collinear limits at the level of cross section factorization: we further discuss this idea in Sec. B.2, which can serve as an additional starting point for parton branching algorithms beyond the leading order⁵.

5.3.1 Quark-gluon splitting

In order to discuss these results in terms of our power counting algorithm, we employ the Sudakov decomposition of Eq. (2.22), *i.e.*

$$\begin{aligned} q_i^\mu &= z_i p_i^\mu + \frac{p_{\perp,i}^2}{z_i 2p_i \cdot n} n^\mu + k_{\perp,i}^\mu, \\ q_j^\mu &= z_j p_i^\mu + \frac{p_{\perp,j}^2}{z_j 2p_i \cdot n} n^\mu + k_{\perp,j}^\mu, \\ q_k^\mu &= z_k p_k^\mu. \end{aligned} \quad (5.17)$$

Using this mapping, we find vertex rules for splitter lines, namely

$$\begin{aligned} \text{Diagram 1} &= \frac{g_s}{S_{ij}} \sqrt{\frac{z_i + z_j}{z_i}} \left(\frac{k_{\perp,i} \not{p}_i}{n \cdot p_i} p_i^\nu - k_{\perp,i} \gamma^\nu \not{p}_i \right), \end{aligned} \quad (5.18a)$$

$$\text{Diagram 2} = 2 \frac{g_s}{S_{ij}} \frac{\sqrt{z_i(z_i + z_j)}}{z_j} \not{p}_i k_{\perp,j}^\nu, \quad (5.18b)$$

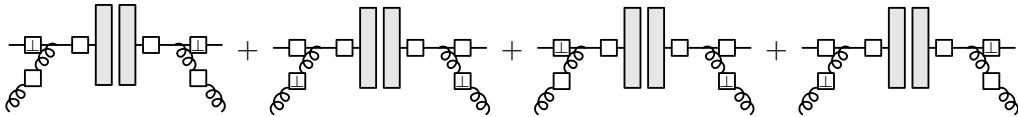
$$\text{Diagram 3} = 2 \frac{g_s}{S_{jk}} z_k \frac{p_i \cdot p_k n^\sigma - n \cdot p_i p_k^\sigma + n \cdot p_k p_i^\sigma}{n \cdot p_i} \not{p}_k, \quad (5.18c)$$

$$\text{Diagram 4} = 2 \frac{g_s}{S_{jk}} \frac{z_k}{z_j} \frac{n \cdot p_k k_{\perp,j}^\sigma + k_{\perp,j} \cdot p_k n^\sigma}{n \cdot p_i} \not{p}_k. \quad (5.18d)$$

The second diagram represents the Eikonal coupling in terms of our mapping. In order to reproduce the splitting function and soft limits, we instate one specific version of the momentum mapping, *i.e.*

$$\begin{aligned} z_i &= z, & z_j &= 1 - z, & z_k &= 1, \\ k_{\perp,i} &= -k_{\perp,k} = k_{\perp}, \\ p_{\perp,i}^2 &= p_{\perp,j}^2 = p_{\perp}^2. \end{aligned} \quad (5.19)$$

Using these rules together with the projectors of Eq. (2.7) for connecting the amplitude and conjugate amplitude, the self-energy like contributions of Eq. (5.12) give



⁵In fact, while we were finalizing the present work, Ref. [31] which discusses a similar question

$$\xrightarrow{\text{Tr}} \frac{4\pi\alpha_s C_F}{S_{ij}} \left[(d-2)(1-z) + \frac{4z^2}{1-z} + 4z \right] \not{p}_i, \quad (5.20)$$

where the soft-singular term in square brackets solely comes about via the second diagram above. In total, we reproduce the well-known spin averaged quark gluon splitting function in $d = 4 - 2\epsilon$ dimensions [28]

$$\langle \hat{P}_{qg}(z) \rangle = C_F \left[\frac{1+z^2}{1-z} - \epsilon(1-z) \right]. \quad (5.21)$$

For the interference contributions of Eq. (5.12), we find

$$\mathbb{P}_{(ij)} \begin{array}{c} \text{---} \square \text{---} \square \text{---} \square \text{---} \\ \text{---} \square \text{---} \square \text{---} \square \text{---} \end{array} = \mathbb{P}_{(ij)} \frac{-4\pi\alpha_s \mathbf{T}_i \cdot \mathbf{T}_k}{S_{ij} S_{jk}} \frac{4z}{1-z} k_\perp \cdot p_k [\not{p}_i][\not{p}_k], \quad (5.22a)$$

$$\mathbb{P}_{(ij)} \begin{array}{c} \text{---} \square \text{---} \square \text{---} \square \text{---} \\ \text{---} \square \text{---} \square \text{---} \square \text{---} \end{array} = \mathbb{P}_{(ij)} \frac{4\pi\alpha_s \mathbf{T}_i \cdot \mathbf{T}_k}{S_{ij} S_{jk}} \frac{4z p_\perp^2}{(1-z)^2} \frac{n \cdot p_k}{n \cdot p_i} [\not{p}_i][\not{p}_k]. \quad (5.22b)$$

Note that one has to include a factor of \sqrt{z} coming from parton i on the conjugate side. Inserting the mapping of Eq. (5.17) in the partitioned version of Eq. (5.15), *i.e.*

$$\mathbb{P}_{(ij)} 8\pi\alpha_s (-\mathbf{T}_i \cdot \mathbf{T}_k) \frac{4}{S_{ij} S_{jk}} \left[q_i \cdot q_k - q_k \cdot q_j \frac{q_i \cdot n}{q_j \cdot n} - q_i \cdot q_j \frac{q_k \cdot n}{q_j \cdot n} \right].$$

This has the same soft limit as Eq. (5.22) (modulo a factor of two from using two times the real part in Eq. (5.15)) This represents a non-trivial check of our power counting rules. Also notice the similarity between Eq. (5.22b) and the soft singular term in Eq. (5.20). We do not have an immediate cancellation between both contributions as was the case for Eq. (5.14) vs. Eq. (5.15). This is due to the fact that we implement the partitioning before carrying out these cancellations and because with each of the three terms in the partitioned Eikonal above containing various powers of soft contributions, these terms mix and we can not isolate each term via a power counting. Nevertheless, when adding up the kernels $\mathbb{U}_{(ij)}$ and $\mathbb{U}_{(jk)}$, Eq. (5.15) is recovered in the soft limit and the soft divergent parts of the splitting functions are cancelled against the respective contributions from the interferences (with the sum over partitioning factors collapsing to 1), leaving only soft interference contributions of the kind in Eq. (5.22a).

Notice that we can, of course, acquire the same behaviour from a different momentum parametrization. In order to show this, it is interesting to look at a momentum mapping with unbalanced (\perp)-component of the emission (in Eq. (5.17), these components are balanced between emittee and emission), because it shows how different contributions in terms of our power counting algorithm lead to the same results. This version of the mapping reads

$$q_i^\mu = z p_i^\mu, \\ q_j^\mu = (1-z) p_i^\mu + \frac{p_\perp^2}{(1-z) 2 p_i \cdot n} n^\mu - k_\perp^\mu,$$

$$\begin{aligned}
& + \text{[diagram 1]} + \text{[diagram 2]} \\
& + \text{[diagram 3]} + \text{[diagram 4]} \\
& + \left(\text{[diagram 5]} + \text{[diagram 6]} + \text{c.c.} \right) \\
& + \left(\text{[diagram 7]} + \text{[diagram 8]} + \text{c.c.} \right) \\
& = \frac{8\pi\alpha_s \mathbf{T}_i^2}{S_{ij}} \left[-2\eta^{\mu\nu} \left(\frac{z}{1-z} + \frac{1-z}{z} \right) + (d-2)z(1-z) \frac{k_\perp^\mu k_\perp^\nu}{p_\perp^2} \right]. \quad (5.31)
\end{aligned}$$

The first term of this expression shows the soft-divergent part of P_{gg} . Turning to the interferences, we have fewer diagrams to take care of because the (\perp)-vertices give soft-subleading contributions. The Eikonal contribution is then given by

$$\begin{aligned}
& \mathbb{P}_{(ij)} \\
& = \mathbb{P}_{(ij)} \frac{8\pi\alpha_s \mathbf{T}_i \cdot \mathbf{T}_k}{S_{ij} S_{jk}} \frac{1+z}{1-z} \frac{n \cdot p_k}{n \cdot p_k + (1-z)n \cdot p_i} p_k \cdot k_\perp \eta^{\mu_i \nu_i} \eta^{\mu_k \nu_k}. \quad (5.32)
\end{aligned}$$

Here, we have used the fact that the hard amplitudes are transverse meaning that terms with a p^{μ_i/ν_i} and p^{μ_k/ν_k} vanish. By the same logic, the leading-soft divergent part is given by

$$\begin{aligned}
& \mathbb{P}_{(ij)} \\
& = \mathbb{P}_{(ij)} \frac{8\pi\alpha_s \mathbf{T}_i \cdot \mathbf{T}_k}{S_{ij} S_{jk}} \frac{p_\perp^2 (1+z)}{(1-z)^2} \frac{(n \cdot p_k)^2}{n \cdot p_i (n \cdot p_k + (1-z)n \cdot p_i)} \eta^{\mu_i \nu_i} \eta^{\mu_k \nu_k}. \quad (5.33)
\end{aligned}$$

5.4 Two emission case

In Tab. 6, we show the leading splitter amplitudes with collinear vertex insertions for all relevant two emission singular configurations, while Tab. 7 shows (\perp)-vertex insertions.

	C_1C_2	C_1S_2	S_1C_2	S_1S_2		C_1C_2	S_1C_2	S_1S_2
	λ^2	λ^2	λ	λ		λ^2	λ	λ
	λ^2	λ^2	λ	λ		λ^2	λ	λ
	λ^2	λ	λ^2	λ		λ^2	λ^2	λ
	λ^2	λ	λ^2	λ		λ^2	λ^2	λ^2
	λ^2	λ	λ	1		λ^2	λ	λ^2
	λ^2	λ^2	λ^2	λ^2		λ^2	λ^2	λ^2
	λ^3	λ^2	λ	λ		λ^3	λ	λ^2
	λ^3	λ^3	λ	λ		λ^3	λ	λ

Table 6: Leading collinear contributions for splitter line with collinear vertices.

In Tab. 8 we show the respective interferer amplitudes. From here, one can deduce the numerator scaling for all relevant two-emission topologies.

These tables feature several noteworthy aspects we want to mention here. Concerning the triple collinear limit ($i \parallel j \parallel k$), we see that many of the splitter amplitudes shown minimally scale as λ^2 . All of these need to be taken into account for this limit while for interferer lines, there is only one relevant amplitude, namely the first one shown in Tab. 8. For self-energy topologies, where one finds a propagator scaling of $1/\lambda^8$ for $E^{(1)}$, $E^{(2)}$ and $E^{(3)}$ this means that the overall scaling drops to $1/\lambda^4$ as one would expect for a contribution to a splitting function. Moreover, we find that these are the *only* relevant topologies for two emission splitting functions as can be seen in Eq. (B.1) and Eq. (B.4).

	C_1C_2	C_1S_2	S_1C_2	S_1S_2		C_1C_2	S_1C_2	S_1S_2
	λ^2	λ^2	λ^2	λ^2		λ^2	λ^2	λ^2
	λ^2	λ^2	λ^2	λ^2		λ^2	λ^2	λ
	λ^2	λ^2	λ^2	λ^2		λ^2	λ^2	λ^2
	λ^2	λ^2	λ	λ		λ^2	λ^2	λ^2
	λ^2	λ	λ^2	λ		λ^2	λ	λ^2
	λ^2	λ^2	λ^2	λ^2		λ^2	λ^2	λ^2

Table 7: Leading collinear contributions for splitter line with transverse vertices.

Instead, for the double soft limit, there is only one amplitude whose numerator does not scale, namely the one with (\perp)-momentum components on the emission lines. This will be the only relevant numerator structure in said limit on the amplitude side. On the interferer side, shown in Tab. 8 all amplitudes shown are relevant, because none of them scale in the double soft-limit. Nevertheless, none of the amplitudes with a (\perp)-vertex shown in Tab. 7 can contribute on the interferer line in a double soft limit, because the inclusion of such a vertex always adds a power of λ to the scaling. This can already be seen in the one emission example, where there are only two relevant interference contributions of Eq. (5.33) and Eq. (5.32) for the same reasons.

Another interesting finding is the appearance of amplitudes with a black box connecting to the hard amplitude. If such an amplitude were to contribute in a leading singular limit, it would be a sign of a factorisation breakdown with the reason being that the backwards components of momenta from the hard amplitude can not be neglected. Nevertheless, a

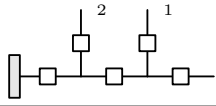
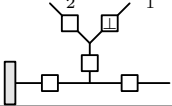
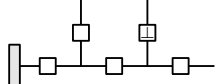
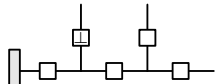
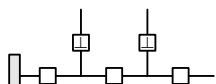
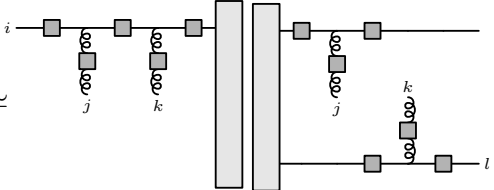
	C_1C_2	C_1S_2	S_1C_2	S_1S_2		C_1C_2	S_1C_2	S_1S_2
	1	1	1	1		λ	1	λ
	λ	λ	1	1				
	λ	1	λ	1				
	λ^2	λ	λ	1				

Table 8: Leading numerator scaling for interferer lines with collinear vertices.

closer inspection of said amplitude shows that in conjunction with the scaling of the relevant partitioning and propagator factors, they do not contribute in any leading singular limit for two emissions.

In general, it is algorithmically an easy task to collect all contributions relevant for a specific leading singularity. One can first check the scaling of partitioning times propagator factors to find potentially relevant topologies (*i.e.* the ones which scale as $1/\lambda^4$ or worse) and then pick the corresponding amplitudes from our lists that feature the lowest scaling in the respective limit. As mentioned in the one emission example, one can finally apply the decomposition of Eq. (2.11) for interferer lines to single out leading soft-singular contributions. We show the scaling of the partitioned propagator factors together with their respective numerator scaling in Tab. 9. All contributions with a scaling of $1/\lambda^4$ should enter the kernel for the collinear configuration in question, in this case the $\mathbb{U}_{(ijk)}$ -kernel. Several remarks for this collection of data are in order. Firstly, we see that only the self-energy like topologies E contribute in the triple collinear limit. For soft-collinear configurations, only a handful of topologies give rise to leading contributions, while almost all of them contribute in the double-soft limit. An interesting difference between the partitioning types is that topology $A^{(3)}$ does not contribute in the double-soft limit for fractional partitioning while it does in the angular ordered version. Both partitionings give rise to the same leading contributions otherwise.

As an illustrative example for a single diagram, we discuss the power counting for the $B^{(1)}$ -topology for the emission of two gluons, *i.e.*

$$B_{ijkl}^{(1)} \simeq \text{Diagram} \propto \frac{1}{S_{ij}^2 S_{ijk} S_{kl}}. \quad (5.34)$$


	CC	CS	SC	SS
$A^{(1)}$	$1/\lambda^2$	$1/\lambda^3$	$1/\lambda$	$1/\lambda^4$
$A^{(2)}$	$1/\lambda^2$	$1/\lambda^2$	$1/\lambda^2$	$1/\lambda^4$
$A^{(3)}$	$1/\lambda^2$	$1/\lambda^2$	$1/\lambda$	$1/\lambda^3$
$A^{(4)}$	$1/\lambda^3$	$1/\lambda^2$	$1/\lambda$	$1/\lambda^4$
$A^{(5)}$	$1/\lambda^3$	$1/\lambda$	$1/\lambda$	$1/\lambda^4$
$B^{(1)}$	$1/\lambda^3$	$1/\lambda^4$	$1/\lambda^2$	$1/\lambda^4$
$B^{(2)}$	$1/\lambda^3$	$1/\lambda^3$	$1/\lambda^3$	$1/\lambda^4$
$B^{(3)}$	$1/\lambda^3$	$1/\lambda^3$	$1/\lambda^2$	$1/\lambda^4$
$B^{(4)}$	$1/\lambda^3$	$1/\lambda^4$	$1/\lambda^2$	$1/\lambda^4$
$B^{(5)}$	$1/\lambda^3$	$1/\lambda^3$	$1/\lambda^3$	$1/\lambda^4$
$B^{(6)}$	$1/\lambda^3$	$1/\lambda^3$	$1/\lambda^2$	$1/\lambda^4$
$X^{(1)}$	$1/\lambda^2$	$1/\lambda^2$	$1/\lambda^4$	$1/\lambda^4$
$X^{(2)}$	$1/\lambda^2$	$1/\lambda^2$	$1/\lambda^2$	$1/\lambda^2$
$E^{(1)}$	$1/\lambda^4$	$1/\lambda^4$	$1/\lambda^2$	$1/\lambda^4$
$E^{(2)}$	$1/\lambda^4$	$1/\lambda^3$	$1/\lambda^3$	$1/\lambda^4$
$E^{(3)}$	$1/\lambda^4$	$1/\lambda^3$	$1/\lambda^2$	$1/\lambda^4$
$E^{(4)}$	$1/\lambda^4$	$1/\lambda^3$	$1/\lambda^2$	$1/\lambda^4$
$E^{(5)}$	$1/\lambda^4$	$1/\lambda^2$	$1/\lambda^2$	$1/\lambda^4$

Table 9: Scaling for propagator times partitioning factor of two emission single emitter topologies when partitioned to $(i \parallel j \parallel k)$ together with the respective numerator scaling. Here, ‘CC’ refers to the triple collinear limit where $i \parallel j \parallel k$, ‘CS’ refers to $(i \parallel j)$ with soft k , ‘SC’ to $(i \parallel k)$ and j soft and ‘SS’ is the double soft limit where both j and k are soft. The leading terms are marked in red.

First, we check the scaling of the diagram’s propagator times the partitioning factors for all limits where the partons j, k can become unresolved explicitly for the partial fractioning version of the partitioning. An example is the triple collinear $(i \parallel j \parallel k)$ -limit. The respective partitioning factor which eliminates the collinear singularity w.r.t. parton l is

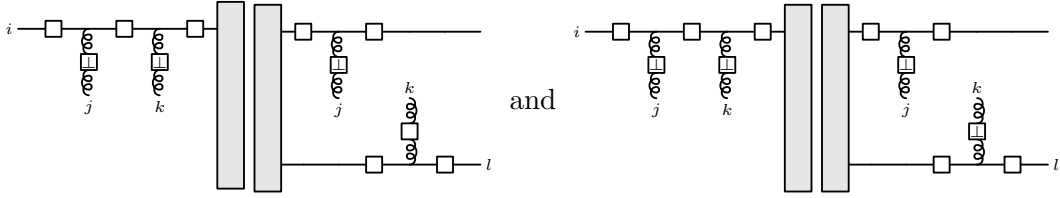
$$\mathbb{P}_{(ijk)}^{B^{(1)}} = \frac{\varsigma^4 S_{kl}}{\varsigma^2 S_{kl} S_{ijk} + \varsigma^4 S_{ijk} + 2S_{ij}^2 S_{ijk} + \varsigma^4 S_{kl}} . \quad (5.35)$$

The configurations c where $\mathbb{P}_c^{B^{(1)}} \times B^{(1)}$ could give rise to a leading singular contribution are shown in Tab. 10. Next, we check the numerator scaling, *i.e.* the possible insertions of subamplitudes from Tab. 6 for the amplitude side and Tab. 5 for the conjugate side. In each case, the (ij) -collinearity leads to a scaling of at least λ^2 for the numerator. Additionally, the (ik) - and (kl) -collinearities give an additional power of λ in the configurations where k is not soft. Then, none of the purely collinear settings give rise to a leading singular contribution (*i.e.* the partitioned amplitude scales as $1/\lambda^n$ with $n < 4$). The only relevant contributions come in the cases where k is soft and j is either collinear to i or also soft from

	$(i \parallel j \parallel k)$	$(i \parallel j)(k \parallel l)$	$(i \parallel j), k \text{ soft}$	$j, k \text{ soft}$
$\mathbb{P}_{(ijk)}^{B^{(1)}}$	$\frac{1}{\lambda^6}$	$\frac{1}{\lambda^4}$	$\frac{1}{\lambda^6}$	$\frac{1}{\lambda^4}$
$\mathbb{P}_{(ij)(kl)}^{B^{(1)}}$	$\frac{1}{\lambda^4}$	$\frac{1}{\lambda^6}$	$\frac{1}{\lambda^6}$	$\frac{1}{\lambda^4}$

Table 10: Leading propagator scalings of $\mathbb{P}_c^{B^{(1)}} \times B^{(1)}$ for four different configurations where the partons j, k can become unresolved.

a partitioning into either $(i \parallel j \parallel k)$ or $(i \parallel j)(k \parallel l)$ (meaning the soft limits in Tab. 10). When applying $\mathbb{P}_{(ijk)}^{B^{(1)}}$ in the double soft limit, there are only two numerator structures which have no λ -scaling and will therefore give rise to a leading contribution, *viz.*



The only other leading contributions appear in the $(i \parallel j)$ and k soft configuration. The relevant numerator structures here are the ones from above and the combinations where the (\perp) -boxes of emission j are moved to one of the nearest neighbour boxes.

In conclusion, we find that, as apparent already from its topology, $B^{(1)}$ contributes leadingly only in the soft-collinear and double soft limits with its only relevant partitions being $\mathbb{P}_{(ijk)}^{B^{(1)}}$ and $\mathbb{P}_{(ij)(kl)}^{B^{(1)}}$.

Two other interesting examples are the $B_{ijkl}^{(2)}$ - and $X_{ijkl}^{(1)}$ -topologies, *i.e.*

$$B_{ijkl}^{(2)} \simeq \text{Diagram} \propto \frac{1}{S_{ij}S_{ik}S_{jk}S_{jl}}, \quad (5.36)$$

and

$$X_{ijkl}^{(1)} \simeq \text{Diagram} \propto \frac{1}{S_{ij}S_{ik}S_{jl}S_{kl}}. \quad (5.37)$$

For $B_{ijkl}^{(2)}$, the same numerator power counting applies as for $B_{ijkl}^{(1)}$. By checking the scaling of its propagator factors times the partitioning, we find that *only* leading singular contribution appears in the double soft limit in $\mathbb{P}_{(ijk)}^{B^{(2)}} B_{ijkl}^{(2)}$. By the same logic, we find that $X_{ijkl}^{(1)}$ exclusively contributes in the double soft limit. The reason in this case is that each partition of $X_{ijkl}^{(1)}$ is at most $1/\lambda^4$ -singular. In any collinear or soft-collinear configuration,

the numerator will contribute at least one power of λ , making these contributions subleading. In the double-soft limit though, each partition (except for the one into $(il)(jk)$) will contribute equally with the respective leading numerator structures being of $\mathcal{O}(1)$.

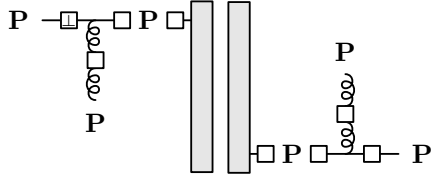
6 Applications and Outlook

In the previous section we have been outlining how one can, given a partitioning of the soft radiation into different collinear sectors, systematically factor the leading behaviour of multi-leg amplitudes. Taking this as a starting point, several applications are in reach: At a fixed order in perturbation theory, one can simply square the amplitude thus obtained, and derive an interpolating formula for the singular behaviour of a fixed number of emissions. While it was not our primary goal to use this as a subtraction term (and we have thus possibly not created functions which are most easily integrated analytically), one can still use the results to migrate certain contributions in between real emission and virtual corrections if there is no immediate need for an analytic integration *e.g.* within the context of the loop-tree duality local subtractions [33, 34] and similar approaches [26].

Within the context of a specific (class of) observables, which exhibit a definite perturbation around a set of hard jets, our findings are a vital input to a resummation programme. In particular, when using azimuthal averaging, and our partitioning which generalizes the subtractions behind angular ordering, we expect that we can obtain a generalization of the coherent branching formalism beyond the usual next-to-leading logarithmic accurate algorithm for global event shapes. Colour correlations can directly be addressed within our analysis and more recent approaches to simplify the structure of colour in the soft limit might be vital to supplement such a formalism, which we will address in future work. An immediate difference of our approach is that we have deliberately not chosen to analytically move soft-collinear contributions in between different classes of diagrams. This implies that the colour-diagonal contributions which involve the same colour charge acting in the amplitude and its conjugate, will still deliver the full soft- and hard-collinear singularity. They do not need to rely on the soft, colour-correlated contribution to collapse into the collinear singularity upon relying on colour conservation. This might be advantageous in a numerical implementation, but also implies that our non-trivially colour correlated contributions truly describe the effect of large-angle soft radiation, which could thus be separated in an analytic way; this should be confronted with the approaches of collinear subtractions outlined in [24]. Within the same parton-branching at the amplitude level approach, our analysis can be exploited to derive splitting kernels beyond the limit of iterated singly-unresolved emissions in order to build up the leading behaviour of an amplitude with many legs. In this case, we will be able to extend the approaches of doubly-unresolved soft radiation [26] to include soft- and hard-collinear limits and thus arrive at a more general algorithm. This is the primary scope of our work, together with the generalized angular-ordered partitioning, as well as the flexible recoil schemes. These allow us to analyse the effect in comparison to previous work in this direction at the level of existing parton branching algorithms [21] for which we are convinced that there will be

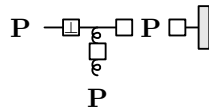
a deeper link established between recoil, partitioning, the form of the evolution kernel and the accuracy of an overall resulting parton branching algorithm.

To be definite, we here give expressions for the factoring vertices in terms of cutting apart the internal lines using the definition of our projector operators in Eq. (2.7), *i.e.* we do contract the vertices which are dressed up with the respective hard, transverse or backward propagator components with polarization vectors and spinors in the respective collinear sectors. From this we obtain (complex) weights for each colour structure, which we can then iterate in a amplitude-level Monte Carlo algorithm. This would in turn, besides the colour quantum numbers, also sample spin quantum numbers. The procedure is sketched below in the case of a gluon emission attaching to a quark splitter and quark spectator line, where the λ and $\bar{\lambda}$ refer to the helicities on the amplitude and conjugate amplitude side, respectively:

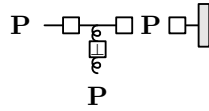


$$\begin{aligned}
& \rightarrow \sum_{\lambda_i, \bar{\lambda}_i} \frac{u_{\lambda_1}}{\sqrt{2n \cdot p_i}} \left[\frac{\bar{u}_{\lambda_1}}{\sqrt{2n \cdot p_i}} \not{k}_{\perp} \not{\epsilon}_{\lambda_3} \not{p}_i \frac{u_{\lambda_2}}{\sqrt{2n \cdot p_i}} \right] \frac{\bar{u}_{\lambda_2}}{\sqrt{2n \cdot p_i}} \epsilon_{\lambda_3}^{\sigma} \\
& \quad \times \frac{u_{\bar{\lambda}_1}}{\sqrt{2n \cdot p_i}} \left[\frac{\bar{u}_{\bar{\lambda}_1}}{\sqrt{2n \cdot p_k}} \not{p}_k \frac{u_{\bar{\lambda}_2}}{\sqrt{2n \cdot p_k}} p_k \cdot \epsilon_{\bar{\lambda}_3} \right] \frac{\bar{u}_{\bar{\lambda}_2}}{\sqrt{2n \cdot p_k}} \epsilon_{\bar{\sigma}, \bar{\lambda}_3}.
\end{aligned} \tag{6.1}$$

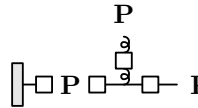
At the end of an evolution built up this way, the amplitude would then be squared by evaluating the matrix element of the final projector corresponding to the most external lines we have been starting with in the first place, and our decomposition and normalization guarantees that there is no need to take into account additional factors. The other vertices we encounter in the case of a single and double emission are outlined below. Here and in the following, the symbol “ \simeq ” stands for only showing the scalar emission quantity that factorizes to the hard amplitude while leaving the rest of the polarization sum and the hard amplitude itself implicit. The relevant expressions for a quark-gluon splitting are



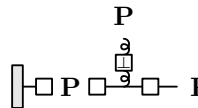
$$\simeq -\frac{g_s}{S_{ij}} \sqrt{\frac{z_i + z_j}{z_i}} \frac{\bar{u}_{\lambda_1}}{\sqrt{2n \cdot p_i}} \left(\not{k}_{\perp, i} \not{\epsilon}_{\lambda_3} \not{p}_i \right) \frac{u_{\lambda_2}}{\sqrt{2n \cdot p_i}}, \tag{6.2a}$$



$$\simeq 2 \frac{g_s}{S_{ij}} \frac{\sqrt{z_i(z_i + z_j)}}{z_j} \frac{\bar{u}_{\lambda_1}}{\sqrt{2n \cdot p_i}} \not{p}_i \frac{u_{\lambda_2}}{\sqrt{2n \cdot p_i}} k_{\perp, j} \cdot \epsilon_{\lambda_3}, \tag{6.2b}$$



$$\simeq -2 \frac{g_s}{S_{jk}} z_k \frac{\bar{u}_{\bar{\lambda}_1}}{\sqrt{2n \cdot p_k}} \left(\not{p}_k p_k \cdot \epsilon_{\bar{\lambda}_3} \right) \frac{u_{\bar{\lambda}_2}}{\sqrt{2n \cdot p_k}}, \tag{6.2c}$$



$$\simeq 2 \frac{g_s}{S_{jk}} \frac{z_k}{z_j} \frac{n \cdot p_k}{n \cdot p_i} \frac{\bar{u}_{\bar{\lambda}_1}}{\sqrt{2n \cdot p_k}} \left(\not{p}_k k_{\perp, j} \cdot \epsilon_{\bar{\lambda}_3} \right) \frac{u_{\bar{\lambda}_2}}{\sqrt{2n \cdot p_k}}. \tag{6.2d}$$

reflect the full set of correlations or to set the framework to derive improved algorithms. In the present work we have set out a framework which starts from the structure of QCD amplitudes using a physical gauge in order to systematically factorize emissions at the level of the density operator, organizing emission kernels through various “key” topologies of collinear splittings. This enabled us to use a power counting and effective set of Feynman rules to determine the singularity structures without resorting to analysing the overlap in between different limits: our algorithm will directly provide an interpolating formula to extract the respective splitting kernels. We have found that the way the kinematics is parametrized and how recoil is handled, has a significant impact on the form of the final kernels and more notably on the possibility to iterate them. This fact is crucial, since one needs to remove iterated strongly ordered emissions from a full kernel addressing the doubly unresolved limits. We have also developed more general partitioning algorithms, which are able to distribute the various interference contributions among leading collinear limits, generalizing both the Catani-Seymour partial fractioning idea as well as a differential version of angular ordering, which effectively subtracts out collinear divergences. We have demonstrated how our partitioning algorithm can be used to distribute the known double-soft behaviour between different classes of contributions, however we stress that this is not our primary strategy to attack the problem of constructing splitting kernels for parton branching algorithms.

Our formalism leads us to branching amplitudes, which carry full spin and colour information and can be used within existing Monte Carlo efforts such as the CVolver [27, 35] framework. One particular fact, which is worth highlighting, is that we keep the hard-collinear behaviour separate in terms of the full splitting function and find that our interference contributions are manifestly suppressed in the collinear limit. We are able to perform this distinction at the expense of an explicit dependence of the gauge vector, for which we have explicitly shown how we can translate this dependence into a backward direction local to each collinear sector. In an upcoming publication we will use the present formalism to outline the full set of double-emission kernels [36]. We also anticipate that a similar formalism, extended to virtual corrections and combined with the techniques presented in [26] will allow us to construct a full second-order evolution at the amplitude level which can be used as a rigorous starting point for improved parton branching algorithms.

Acknowledgements

The work of ML is supported partially by the DFG Collaborative Research Center TRR 257 “Particle Physics Phenomenology after the Higgs Discovery”. ESD has been supported by the Marie Skłodowska-Curie Innovative Training Network MCnetITN3 (grant agreement no. 722104). This work has also been supported in part by the COST actions CA16201 “PARTICLEFACE” and CA16108 “VBSCAN”. We are grateful to the Erwin Schrödinger Institute Vienna for hospitality and support while significant parts of this work have been achieved within the Research in Teams programmes “Higher-order Corrections to Parton Branching at the Amplitude Level” (RIT2020) and “Amplitude Level Evolution I: Initial

State Evolution.” (RIT0421). We are deeply obliged to Stefan Gieseke for his trust and support, and we would like to thank Jeffrey Forshaw, Jack Holguin, Kirill Melnikov, Ines Ruffa and Malin Sjö Dahl for fruitful discussions.

A Phase space factorization

In this section, we discuss how phase space factorisation is achieved with a generic version of the momentum mapping of Sec. 4. Compared to the discussion of various momentum mappings in [37], we face the difficulty of treating collinear and soft configurations simultaneously, together with a global Lorentz-transformation. The latter can have a non-trivial dependence on emission and progenitor momenta, which needs to be carefully traced when switching integration variables. In the following, we will use the notation

$$[dq] \equiv \frac{d^d q}{(2\pi)^{d-1}} \delta(q^2) \Theta(q^0). \quad (\text{A.1})$$

We are interested in the phase space

$$\text{PS} = \delta^{(d)} \left(\sum_i q_i + K - Q \right) \prod_i [dq_i] \prod_l [dk_{i,l}], \quad (\text{A.2})$$

where K is the sum over all emission momenta $k_{i,l}$, Q is the overall momentum transfer and we think of the q_i as emitter and recoiler momenta. The goal is to express this phase space in terms of the progenitor momenta p_i of an emission process.

A.1 Emission phase space

We begin the discussion with a generic version of the emission momenta, *i.e.*

$$k_{il}^\mu = \frac{1}{\hat{\alpha}} \Lambda^\mu{}_\nu \hat{k}_{il}^\nu, \quad \hat{k}_{il}^\nu = \alpha_{il} p_i^\nu + \beta_{il} n^\nu + k_{\perp,il}^\nu. \quad (\text{A.3})$$

The Lorentz-transformation Λ and scaling factor $\hat{\alpha}$ will be functions of p_i , n , α_{il} , β_{il} and $k_{\perp,il}$. The use of a local backwards direction n_i will be discussed in the next section. We fix this mapping by inserting

$$\begin{aligned} [dk_{il}] &= [dk_{il}] \times \delta \left(\alpha_{il} - \frac{1}{\hat{\alpha}} \frac{(\Lambda n) \cdot k_{il}}{n \cdot p_i} \right) d\alpha_{il} \\ &\times \delta \left(\beta_{il} - \frac{1}{\hat{\alpha}} \frac{(\Lambda p_i) \cdot k_{il}}{n \cdot p_i} - \frac{p \cdot k_{\perp,il}}{n \cdot p_i} \right) d\beta_{il} \\ &\times \delta \left(k_{\perp,il} - \alpha \Lambda^{(-1)} k_{il} + \alpha_{il} p_i + \beta_{il} n \right) d^d k_{\perp,il}. \end{aligned} \quad (\text{A.4})$$

Now, we switch the integration from $k_{il} \rightarrow \hat{k}_{il}$, use the fact that $\Lambda \in SO^+(1,3)$ and assume $n^2 = 0$ and $n \cdot p_i > 0$. This yields

$$\begin{aligned} [dk_{il}] &= \hat{\alpha}^{2-d} [d\hat{k}_{il}] \times \delta \left(\alpha_{il} - \frac{n \cdot \hat{k}_{il}}{n \cdot p_i} \right) d\alpha_{il} \\ &\times \delta \left(\beta_{il} - \frac{p_i \cdot \hat{k}_{il}}{n \cdot p_i} - \frac{p_i \cdot k_{\perp,il}}{n \cdot p_i} \right) d\beta_{il} \\ &\times \delta \left(\hat{k}_{il} - \alpha_{il} p_i - \beta_{il} n - k_{\perp,il} \right) d^d k_{\perp,il} \end{aligned} \quad (\text{A.5})$$

and we can remove the integration $d^d \hat{k}_{il}$ via the last Dirac-delta. This also fixes the projections of n and p_i on \hat{k}_{il} and we can replace

$$\begin{aligned}\frac{n \cdot \hat{k}_{il}}{n \cdot p_i} &= \alpha_{il} + \frac{n \cdot k_{\perp,il}}{n \cdot p_i} \\ \frac{p_i \cdot \hat{k}_{il}}{n \cdot p_i} &= \beta_{il} + \frac{p_i \cdot k_{\perp,il}}{n \cdot p_i} + \alpha_{il} \frac{p_i^2}{n \cdot p_i}.\end{aligned}\tag{A.6}$$

in Eq. (A.5). Moreover, we have

$$\delta(\hat{k}_{il}^2) = \delta(\alpha_{il}(\alpha_{il} p_i^2 + 2p_i \cdot k_{\perp,il}) + 2\beta_{il} n \cdot k_{\perp,il} + k_{\perp,il}^2 + \beta_{il} 2\alpha_{il} p_i \cdot n)\tag{A.7}$$

Using the remaining delta-functions in Eq. (A.5) and carrying out the β_{il} -integration then fixes

$$\beta_{il} = \frac{-k_{\perp,il}^2}{\alpha_{il} 2n \cdot p_i}.\tag{A.8}$$

This leads to

$$\begin{aligned}[dk_{il}] &= \frac{\hat{\alpha}^{2-d}}{(2\pi)^{d-1}} \frac{n \cdot p_i}{2\alpha_{il}} \delta(n \cdot k_{\perp,il}) \delta(\alpha_{il} p_i^2 + 2p_i \cdot k_{\perp,il}) \\ &\times \Theta\left(\alpha_{il} p_i^0 + \frac{-k_{\perp,il}^2}{\alpha_{il} 2n \cdot p_i} n^0 + k_{\perp,il}^0\right) d\alpha_{il} d^d k_{\perp,il}.\end{aligned}\tag{A.9}$$

One can now consider a frame where p_i and n are back to back and rewrite the $k_{\perp,il}$ -integration in terms of polar coordinates. What we then find is

$$[dk_{il}] = \frac{\hat{\alpha}^{2-d}}{2\alpha_{il}} d\alpha_{il} p_{\perp,il}^{d-3} dp_{\perp,il} d\Omega^{(d-3)} \Theta(p_{\perp,il}) \Theta(\alpha_{il}),\tag{A.10}$$

with the properties

$$\begin{aligned}k_{\perp,il} \cdot n &= 0, \quad k_{\perp,il} \cdot p_i = -\frac{\alpha_{il} p_i^2}{2} \\ k_{\perp,il}^2 &= -p_{\perp,il}^2, \quad \beta_{il} = \frac{p_{\perp,il}^2}{\alpha_{il} 2p_i \cdot n}.\end{aligned}\tag{A.11}$$

A.2 Emitter and recoiler phase space

For the discussion of the emitter and recoiler phase space, we use

$$q_i^\mu = \frac{1}{\hat{\alpha}} \Lambda^\mu{}_\nu \hat{q}_i^\nu,\tag{A.12}$$

and discuss some details related to the introduction of the Lorentz-transformation. First, we consider the momentum conserving delta-function of Eq. (A.2). Inserting the transformed momenta, we demand

$$\delta^{(d)}\left(\frac{\Lambda}{\hat{\alpha}} \sum_i (\hat{q}_i + \sum_l \hat{k}_{il}) - Q\right) = \delta^{(d)}\left(\frac{\Lambda}{\hat{\alpha}} (P - Q)\right),\tag{A.13}$$

where $P = \sum_i p_i$. This is achieved by choosing the Lorentz transformation such that

$$\Lambda^\mu{}_\nu \frac{Q^\nu + N^\nu}{\hat{\alpha}} = Q^\mu, \quad (\text{A.14})$$

with

$$N = \sum_i \left(\hat{q}_i + \sum_l \hat{k}_{il} - p_i \right), \quad (\text{A.15})$$

and

$$\hat{\alpha} = \sqrt{\frac{(Q + N)^2}{Q^2}}. \quad (\text{A.16})$$

Explicitly, this Lorentz-transformation reads [28]

$$\Lambda^\mu{}_\nu(p_1 \rightarrow p_2) = \eta^\mu{}_\nu - \frac{2(p_1 + p_2)^\mu (p_1 + p_2)_\nu}{(p_1 + p_2)^2} + \frac{2p_2^\mu p_{1\nu}}{p_1^2}. \quad (\text{A.17})$$

Due to Λ being a function of the p_i , *i.e.* via $N = N(\{p_i\})$, one could in principle find derivative terms of the transformation when applying the usual transformation laws for Dirac delta-functions. As it turns out though, we find

$$\frac{\partial}{\partial p_j^\rho} \left(\frac{\Lambda^\mu{}_\nu}{\hat{\alpha}} (P^\mu - Q^\mu) \right) \Big|_{P=Q} = \frac{\Lambda^\mu{}_\rho}{\hat{\alpha}} \Big|_{P=Q}. \quad (\text{A.18})$$

This means that with Λ having a unit determinant, we find

$$\delta^{(d)} \left(\frac{\Lambda}{\hat{\alpha}} (P - Q) \right) = \hat{\alpha}^d \delta(P - Q). \quad (\text{A.19})$$

Next, we discuss the variable change in $[dq_i] \rightarrow [dp_i]$. In order to study the p_i -dependence in the emitter and recoiler momenta, we define

$$\hat{q}_i^\nu = (1 - A_i) p_i^\nu - R_i, \quad (\text{A.20})$$

where R_i depends on the choice of a recoil scheme:

$$R_i = \begin{cases} B_i n_i + K_{\perp,i} & (\text{balanced}) \\ 0 & (\text{unbalanced}) \end{cases} \quad (\text{A.21})$$

Demanding

$$\hat{q}_i^2 = (1 - A_i) p_i^2 \quad (\text{A.22})$$

leads to

$$B_i = -\frac{1}{2n_i \cdot p_i} \left(\frac{K_{\perp,i}^2}{1 - A_i} + 2K_{\perp,i} \cdot p_i \right). \quad (\text{A.23})$$

We note that the R_i , as well as $\hat{\alpha}$ and Λ can be functions of the α_{il} , $p_{\perp,il}$, Ω_{il} and p_i . Therefore, we again need to study this dependence when switching integration variables.

$$d^d q_i = \det \mathcal{J}(\{q_i\}, \{p_i\}) d^d p_i. \quad (\text{A.24})$$

For the Jacobian, we find

$$\mathcal{J}(\{q_i\}, \{p_i\}) = \frac{\partial q_i^\mu}{\partial p_j^\rho} = \frac{\Lambda^\lambda}{\hat{\alpha}} \left[\underbrace{\hat{\alpha} \Lambda^\xi_\mu \frac{\partial}{\partial N^\sigma} \left(\frac{\Lambda^\mu_\nu}{\hat{\alpha}} \right) \frac{\partial N^\sigma}{\partial p_j^\rho} \hat{q}_i^\nu + \frac{\partial \hat{q}_i^\xi}{\partial p_j^\rho}}_{=\hat{\mathcal{J}}} \right]. \quad (\text{A.25})$$

We can now use

$$N = \begin{cases} \sum_i (\sum_l \beta_{il} - B_i) n_i & (\text{balanced}) \\ \sum_i (\sum_l \beta_{il} n_i + K_{\perp,i}) & (\text{unbalanced}). \end{cases} \quad (\text{A.26})$$

In both cases, N has a uniform soft and collinear scaling. For a global n , this shows that the derivative terms in $\hat{\mathcal{J}}$ can be neglected and we have

$$\frac{\partial \hat{q}_i^\mu}{\partial p_j^\nu} = (1 - A_i) \delta_{ij} \delta^\mu_\nu + \mathcal{O}(\lambda). \quad (\text{A.27})$$

This means we have

$$d^d q_i = \hat{\alpha}^{-d} (1 - A_i)^d d^d p_i + \mathcal{O}(\lambda). \quad (\text{A.28})$$

The p_i -dependence for the case of a local n_i is more involved, but we expect the general features of this discussion to hold in that case as well. Lastly, the delta-function for the on-shell condition of the q_i is

$$\delta(q_i^2) = \frac{\hat{\alpha}^2}{(1 - A_i)^2} \delta(p_i^2). \quad (\text{A.29})$$

Putting everything together, we have

$$[dq_i] = \left(\frac{\hat{\alpha}}{1 - A_i} \right)^{2-d} \delta(p_i^2) \Theta[(1 - A_i)p_i^0 - R_i^0] \frac{d^d p_i}{(2\pi)^{d-1}} + \mathcal{O}(\lambda). \quad (\text{A.30})$$

In the unbalanced case, where $R_i = 0$, the Heaviside function immediately leads to an upper bound for A_i . The same is true for the balanced case, but in a less obvious way due to the more involved additional dependence on $K_{\perp,i}$.

Note that Eq. (A.30) shows a powerful result: switching from a momentum mapping with a global gauge vector n to one with a local n_i only amounts to a redefinition of $k_{\perp,il}$ via Eq. (2.41) in Eq. (A.9) because additional modifications only amount to subleading power.

B Two emissions

B.1 Quark-gluon-gluon splitting function

In this section, we want to demonstrate how the two-emission splitting function $\langle \hat{P}_{g_1 g_2 q} \rangle$ for the emission of two gluons off of a quark comes about in our formalism. For brevity, we show the results in terms of cut diagrams, which can be acquired via tracing over the amplitude insertions from Tab. 6 with the lowest numerator scaling.

First, we note that in lightcone gauge all interference contributions are subleading in the collinear limit. Therefore, the splitting function is fully contained in the self energy-like diagrams. Note that using our power counting rules, one immediately sees that only the forward component of the off-shell lines connecting to the hard amplitude give rise to leading contributions.

The Abelian part of the splitting function is given by

$$\begin{aligned}
& \frac{\mu^{4\epsilon}}{\hat{\alpha}^2} \left\{ \left[\text{Diagram 1} + \left(\text{Diagram 2} + (1 \leftrightarrow 2) \right) \right] \right\}_{C_F^2} \\
& = \left(\frac{8\pi\alpha_S}{\hat{\alpha}S_{i12}} \mu^{2\epsilon} \right)^2 C_F^2 \langle \hat{P}_{ggq}^{(\text{Ab})} \rangle \hat{p}_i + \mathcal{O}(\beta_{il}^{-3/2}). \tag{B.1}
\end{aligned}$$

The subscript on the curly brackets stands for an extraction of terms proportional to C_F^2 . This is necessary because the second diagram has the colour structure

$$T^a T^b T^a T^b = \left(C_F^2 - \frac{1}{2} C_A C_F \right) \mathbf{1}_N. \tag{B.2}$$

Therefore, it also contributes to the non-Abelian part of the splitting function. The splitting function in terms of our momentum mapping then reads

$$\begin{aligned}
\frac{\langle \hat{P}_{ggq}^{(\text{Ab})} \rangle}{4S_{i12}^2} & = \frac{1-\epsilon}{2S_{i12}^2} \left\{ 2 - (1-\epsilon) \frac{(S_{i1} + S_{i2})^2}{S_{i1}S_{i2}} \right\} \\
& + \frac{1}{2S_{i1}S_{i2}} \left\{ - (1-\epsilon)^2 (1-A_i) + \frac{(1-\epsilon)(1-A_i)(A_i^2 + \alpha_{i1}\alpha_{i2}) + 2(1-A_i)^2}{\alpha_{i1}\alpha_{i2}} \right\} \\
& + \frac{1}{S_{i1}S_{i12}} \left\{ (1-\epsilon)^2 (2-A_i) + \frac{(1-\epsilon)[2(A_i-2)\alpha_{i1}\alpha_{i2} + (1-\alpha_{i2})(A_i^2 - \alpha_{i1}\alpha_{i2})]}{\alpha_{i1}\alpha_{i2}} \right. \\
& \quad \left. + \frac{(1-A_i)(1-\alpha_{i2})}{\alpha_{i1}\alpha_{i2}} \right\} + (1 \leftrightarrow 2) \tag{B.3}
\end{aligned}$$

The non-Abelian part comes about via

$$\begin{aligned}
& \frac{\mu^{2\epsilon}}{\hat{\alpha}^2} \left\{ \left[\text{Diagram 1} + \left(\text{Diagram 2} + \text{Diagram 3} + \text{Diagram 4} + (1 \leftrightarrow 2) \right) \right] \right\}_{C_A C_F}
\end{aligned}$$

$$= \left(\frac{8\pi\alpha_S}{\hat{\alpha}S_{i12}} \mu^{2\varepsilon} \right)^2 C_A C_F \langle \hat{P}_{ggq}^{(\text{nAb})} \rangle \hat{p}_i + \mathcal{O}(\beta_{il}^{-3/2}), \quad (\text{B.4})$$

with

$$\begin{aligned} \frac{\langle \hat{P}_{ggq}^{(\text{nAb})} \rangle}{4S_{i12}^2} &= \frac{1}{S_{i12}^2} \left\{ \frac{(1-\varepsilon)^2}{2} - \frac{(1-\varepsilon)[\alpha_{i1}(S_{i2}+S_{12}) - \alpha_{i2}S_{i1}][\alpha_{i2}(S_{i1}+S_{12}) - \alpha_{i1}S_{i2}]}{S_{i2}^2 A_i^2} \right\} \\ &+ \frac{1}{S_{i2}S_{i2} A_i \alpha_{i1}} \left\{ (1-\alpha_{i1})\alpha_{i1} + (1-A_i)A_i + \frac{(1-\varepsilon)}{2}(\alpha_{i1}^3 + A_i^3) \right\} \\ &+ \frac{1}{2S_{i1}S_{i2}} \left\{ \frac{(1-\varepsilon)^2}{2}(1-A_i) - \frac{(1-\varepsilon)(1-A_i)(\alpha_{i1}\alpha_{i2} + A_i^2)}{\alpha_{i1}\alpha_{i2}} - \frac{(1-A_i)^2}{\alpha_{i1}\alpha_{i2}} \right\} \\ &+ \frac{1}{S_{i2}S_{i12} A_i \alpha_{i1}} \left\{ \frac{(1-\varepsilon)}{2}[\alpha_{i,1}^3 - \alpha_{i,2}^3 - 2\alpha_{i,1}(\alpha_{i,1} - \alpha_{i,2})] \right. \\ &\quad \left. + (2A_i - 3)\alpha_{i1} - A_i\alpha_{i2} + \alpha_{i2} \right\} \\ &+ \frac{1}{2S_{i2}S_{i12}} \left\{ \frac{(1-\varepsilon)^2}{2}(\alpha_{i1} - 1) + \frac{(1-\varepsilon)(\alpha_{i1} - 1)(\alpha_{i1}^2 - \alpha_{i2}\alpha_{i1} - \alpha_{i2}^2)}{\alpha_{i2}A_i} \right. \\ &\quad \left. - \frac{\alpha_{i1}^2 - 2\alpha_{i1} + 1}{\alpha_{i2}A_i} \right\} + (1 \leftrightarrow 2). \end{aligned} \quad (\text{B.5})$$

Note that the first diagram has the topology of E_1 , see Fig. 6. Using the identifications

$$z_2 = \alpha_{i1}, \quad z_1 = \alpha_{i2}, \quad z_3 = 1 - A_i = 1 - \alpha_{i1} - \alpha_{i2}, \quad (\text{B.6})$$

$$s_{123} = S_{i12}, \quad s_{13} = S_{i2} \text{ etc.}, \quad (\text{B.7})$$

one can verify that the splitting function from Eq. (B.1) and Eq. (B.4) coincide with the well known ones as presented in [38].

B.2 Relation to soft and soft-collinear functions

In this section, we want to study the interplay of soft divergent terms for two emissions as an extension of what we discussed in Sec. 5.3. For this purpose, we investigate the composition of the two-emission splitting function and check its relation to the double soft and soft-collinear results of [38] by taking its soft-soft and soft-collinear limits. For comparability, we use a notation in terms of dot-products to stay independent of a momentum mapping, *e.g.* $\alpha_{i1} = n \cdot q_1$. Also note that in the following, partons 1 and 2 are switched as compared to Eq. (B.1) for an easier translation of our results to the ones of [38].

Double soft limit

Of specific interest is the behaviour of the splitting function in the double soft limit where the Abelian part should reproduce the double Eikonal function and the non-Abelian part the two-gluon soft function $\mathcal{S}_{ij}(q_1, q_2)$.

First, we make use of the following scaling behaviour in the soft-soft limit:

$$S_{12} \rightarrow \lambda^2 S_{12}, \quad S_{i(1/2)} \rightarrow \lambda S_{i(1/2)}, \quad n \cdot q_{1/2} \rightarrow \lambda n \cdot q_{1/2} \quad (\text{B.8})$$

Then, the splitting function has the following leading soft terms:

$$\begin{aligned} \left. \frac{\langle \hat{P}_{q_i q_1 q_2}^{(\text{Ab})} \rangle}{S_{i12}^2} \right|_{SS} &= \frac{S_{i2} + 3S_{i1}}{S_{i2} S_{i1} (S_{i1} + S_{i2})} \frac{(n \cdot q_i)^2}{(n \cdot q_1)(n \cdot q_2)} + (1 \leftrightarrow 2) = \frac{4}{S_{i2} S_{i1}} \frac{(n \cdot q_i)^2}{(n \cdot q_1)(n \cdot q_2)}, \\ \left. \frac{\langle \hat{P}_{q_i q_1 q_2}^{(\text{nAb})} \rangle}{S_{i12}^2} \right|_{SS} &= \frac{1}{S_{12} S_{i1}} \frac{n \cdot q_i (n \cdot q_1 + 2n \cdot q_2)}{n \cdot q_2 (n \cdot q_1 + n \cdot q_2)} - \frac{1}{S_{i1} S_{i2}} \frac{(n \cdot q_i)^2}{2(n \cdot q_1)(n \cdot q_2)} \\ &\quad \frac{1}{(S_{i1} + S_{i2})(n \cdot q_1 + n \cdot q_2)} \left[\frac{1}{S_{12}} \frac{n \cdot q_i (n \cdot q_1 - 3n \cdot q_2)}{n \cdot q_2} - \frac{1}{S_{i1}} \frac{(n \cdot q_i)^2}{n \cdot q_1} \right] \\ &\quad + \frac{1 - \varepsilon}{S_{12}^2} \frac{(n \cdot q_1 S_{i2} - n \cdot q_2 S_{i1})^2}{(S_{i1} + S_{i2})^2 (n \cdot q_1 + n \cdot q_2)^2} + (1 \leftrightarrow 2). \end{aligned} \quad (\text{B.9})$$

The amplitude factorises in the soft limit with a factor of the two gluon soft current, $J_{\mu_1 \mu_2}^{a_1 a_2}(q_1, q_2)$, which contains the double Eikonal and the two-gluon soft function. For the squared amplitude the factor can be simplified into the following form [38]:

$$\begin{aligned} [J_{\mu\rho}^{a_1 a_2}(q_1, q_2)]^\dagger d^{\mu\nu}(q_1) d^{\rho\sigma}(q_2) J_{\nu\sigma}^{a_1 a_2}(q_1, q_2) \\ = \frac{1}{2} \{ \mathbf{J}^2(q_1), \mathbf{J}^2(q_2) \} - C_A \sum_{i,j=3}^n \mathbf{T}_i \cdot \mathbf{T}_j \mathcal{S}_{ij}(q_1, q_2) + \dots \end{aligned} \quad (\text{B.10})$$

where additional terms vanish in combination with the factorised amplitude as they are proportional to the total colour charge. The first term is the anti-commutator of the single emission squared gluon current of Eq. (5.15). It can be written as

$$\frac{1}{2} \{ \mathbf{J}^2(q_1), \mathbf{J}^2(q_2) \} = \frac{1}{2} \sum_{i,j} \sum_{k,l} [(\mathbf{T}_i \cdot \mathbf{T}_j)(\mathbf{T}_k \cdot \mathbf{T}_l) + (\mathbf{T}_k \cdot \mathbf{T}_l)(\mathbf{T}_i \cdot \mathbf{T}_j)] \frac{4S_{ij}^2}{S_{i1} S_{j1} S_{k2} S_{l2}}. \quad (\text{B.11})$$

The second term contains the two-gluon soft function which can be written as

$$\begin{aligned} \mathcal{S}_{ij}(q_1, q_2) = 2 \left\{ \frac{1}{S_{12} S_{i1}} \frac{p_j \cdot q_i (p_j \cdot q_1 + 2p_j \cdot q_2)}{p_j \cdot q_2 (p_j \cdot q_1 + p_j \cdot q_2)} - \frac{1}{S_{i1} S_{i2}} \frac{(p_j \cdot q_i)^2}{2(p_j \cdot q_1)(p_j \cdot q_2)} \right. \\ + \frac{1}{(S_{i1} + S_{i2})(p_j \cdot q_1 + p_j \cdot q_2)} \left[\frac{1}{S_{12}} \frac{p_j \cdot q_i (p_j \cdot q_1 - 3p_j \cdot q_2)}{p_j \cdot q_2} - \frac{1}{S_{i1}} \frac{(p_j \cdot q_i)^2}{p_j \cdot q_1} \right] \\ + \frac{1 - \varepsilon}{S_{12}^2} \left[\frac{(p_j \cdot q_1 S_{i2} - p_j \cdot q_2 S_{i1})^2}{(S_{i1} + S_{i2})^2 (p_j \cdot q_1 + p_j \cdot q_2)^2} + \frac{S_{i1} S_{i2}}{(S_{i1} + S_{i2})^2} + \frac{(p_j \cdot q_1)(p_j \cdot q_2)}{(p_j \cdot q_1 + p_j \cdot q_2)^2} \right] \left. \right\} \\ + (1 \leftrightarrow 2). \end{aligned} \quad (\text{B.12})$$

Note that the last two terms vanish when inserted into Eq. (B.10) and colour-conservation is applied, because they do not depend on either the parton labels i or j . Using the gauge-independence of the splitting function and choosing $n = p_j$ shows an exact correspondence

of the functional dependencies between Eq. (B.12) and two times the non-Abelian part of Eq. (B.9). It therefore exhibits the overlap between the soft singular bits of the splitting function and the two gluon soft current squared.

We can now go one step further and apply our partitioning algorithm to Eq. (B.11) and Eq. (B.12). For the Abelian part of Eq. (B.11), we realize that for partons $k = i$ and $l = j$, the propagator factors are given exactly by the ones of the $X^{(1)}$ -topology shown in App. C which leads to

$$\frac{1}{2}\{\mathbf{J}^2(q_1), \mathbf{J}^2(q_2)\} = \sum_{i,j} [(\mathbf{T}_i \cdot \mathbf{T}_j)^2] \mathcal{P}(X_{i12j}^{(1)}) \times 4S_{ij}^2, \quad (\text{B.13})$$

where $\mathcal{P}(X_{i12j}^{(1)})$ are the respective propagator factors. This means that we can partition this contribution into different collinear sectors with any of the two partitioning variants of Sec. 3. Note that the terms where $k \neq i$ and $l \neq j$ can be viewed as as single emission squared contributions. The same option presents itself for the non-Abelian part, Eq. (B.12), when rewriting the scalar products in terms of S -invariants and using the fact that we can introduce the triple invariants S_{i12} and S_{j12} via

$$S_{i1} + S_{i2} = S_{i12}N_{i12} = S_{i12}(1 + \mathcal{O}(\lambda^2)), \quad N_{i12} = \frac{S_{i1} + S_{i2}}{S_{i12}}. \quad (\text{B.14})$$

The result is

$$\begin{aligned} \mathcal{S}_{ij}(q_1, q_2) = & \mathcal{P}(B_{i1j2}^{(4)}) \times 2S_{ij}(S_{j1} + 2S_{j2})N_{j12} - \mathcal{P}(X_{i12j}^{(1)}) \times S_{ij}^2 \\ & + \mathcal{P}(A_{i12j}^{(3)}) \times 2S_{ij}(S_{j1} - 3S_{j2})N_{i12}N_{j12} - \mathcal{P}(A_{i12j}^{(2)}) \times 2S_{ij}^2N_{i12}N_{j12} \\ & + \mathcal{P}(A_{i12j}^{(5)}) \times 2(1 - \varepsilon)(S_{i1}S_{j2} + S_{i2}S_{j1})N_{i12}N_{j12} + (1 \leftrightarrow 2). \end{aligned} \quad (\text{B.15})$$

Having extracted these propagator factors and realizing that each of them corresponds to a known topology, we again can apply partitionings into different collinear sectors for each term.

What we have just shown presents an alternative way of building up a splitting operator compared to what we discuss in the main part of this work. The procedure of constructing a splitting operator for some specific collinear setting, *e.g.* ($i \parallel 1 \parallel 2$), would be as follows:

1. Extract double soft and soft-collinear (shown in the next subsection) bits of the splitting function by using its gauge-independence, *i.e.* by choosing a reference (recoiler) momentum and comparing to the known soft-limits. The leftover parts can be viewed as purely collinear-singular ones for some specific collinear setting.
2. Recombine the partitioned soft and soft-collinear bits for said collinear setting with the purely collinear bits.
3. The resulting object reproduces the original collinear behaviour of the splitting function (because the partitioning does not spoil the scaling), but do not contribute in other collinear sectors due to the partitioning. The correct soft and soft-collinear behaviour is reproduced when summing up the splitting operators of the different collinear sectors, because the partitioning is build up simply as a decomposition of unity.

Soft-collinear limit

The two emission splitting function shows very similar relations in the soft-collinear limit. The soft-collinear scaling where q_1 is collinear to q_i and q_2 is soft (which we denote as $\dots|_{S_2C_{i1}}$) is as follows:

$$S_{12} \rightarrow \lambda S_{12}, \quad S_{i2} \rightarrow \lambda S_{i2}, \quad S_{i1} \rightarrow \lambda^2 S_{i1}, \quad n \cdot q_2 \rightarrow \lambda n \cdot q_2. \quad (\text{B.16})$$

The splitting function in this limit has the form

$$\begin{aligned} \left. \frac{\langle \hat{P}_{q_i g_1 g_2} \rangle}{S_{i12}^2} \right|_{S_2C_{i1}} &= C_F \frac{(n \cdot q_1)^2 (1 - \varepsilon) + 2(n \cdot q_i)^2 + 2(n \cdot q_1)(n \cdot q_i)}{S_{i1}(n \cdot q_1)(n \cdot q_1 + n \cdot q_i)} \\ &\times \left\{ C_F \left[\frac{n \cdot q_1 + n \cdot q_i}{(S_{12} + S_{i2})n \cdot q_2} + \frac{n \cdot q_i}{S_{i2} n \cdot q_2} \right] - \frac{C_A}{2} \left[\frac{n \cdot q_i}{S_{i2} n \cdot q_2} - \frac{n \cdot q_1}{S_{12} n \cdot q_2} \right] \right\}. \end{aligned} \quad (\text{B.17})$$

At the same time, we know that the factorised squared amplitude in the soft-collinear limit can be written as [38]:

$$\begin{aligned} &|\mathcal{M}_{g, a_1, a_2, \dots, a_n}(q, p_1, p_2, \dots, p_n)|^2 \\ &\simeq -\frac{2}{S_{12}} (4\pi\mu^{2\varepsilon}\alpha_s)^2 \langle \mathcal{M}_{a, \dots, a_n}(p, \dots, p_n) | \hat{\mathbf{P}}_{a_1, a_2}[\mathbf{J}_{(12)\mu}^\dagger(q)\mathbf{J}_{(12)}^\mu(q)] | \mathcal{M}_{a, \dots, a_n}(p, \dots, p_n) \rangle, \end{aligned} \quad (\text{B.18})$$

where

$$\mathbf{J}_{(12)\mu}^\dagger(q)\mathbf{J}_{(12)}^\mu(q) \simeq \sum_{i,j=3}^n \mathbf{T}_i \cdot \mathbf{T}_j \mathcal{S}_{ij}(q) + 2 \sum_{i=3}^n \mathbf{T}_i \cdot \mathbf{T}_{(12)} \mathcal{S}_{i(12)}(q), \quad (\text{B.19})$$

and

$$\mathbf{T}_{(12)} = \mathbf{T}_1 + \mathbf{T}_2. \quad (\text{B.20})$$

The Eikonal functions of the soft emissions are defined as

$$\mathcal{S}_{ij}(q) = \frac{2S_{ij}}{S_{iq}S_{jq}}, \quad \mathcal{S}_{i(12)}(q) = \frac{2(S_{i1} + S_{i2})}{S_{iq}(S_{1q} + S_{2q})}. \quad (\text{B.21})$$

Note that the first factor in Eq. (B.17) exactly coincides with the single emission splitting function $\langle \hat{P}_{q_i g_1}(z_i) \rangle / S_{i1}$ for

$$z_i = \frac{n \cdot q_i}{n \cdot q_1 + n \cdot q_i}. \quad (\text{B.22})$$

As in the double-soft case, we can now set $n = p_j$ in Eq. (B.17) to find

$$\left. \frac{\langle \hat{P}_{q_i g_1 g_2} \rangle}{S_{i12}^2} \right|_{S_2C_{i1}} = \frac{\langle \hat{P}_{q_i g_1}(z_i) \rangle}{2S_{i1}} \left\{ C_F [\mathcal{S}_{ij}(q_2) + \mathcal{S}_{j(i1)}(q_2)] - \frac{C_A}{2} [\mathcal{S}_{ij}(q_2) - \mathcal{S}_{1j}(q_2)] \right\}. \quad (\text{B.23})$$

This shows how the genuine soft-collinear behaviour as described by Eq. (B.18) can be reproduced via the two-emission splitting function (up to the correct reproduction of the colour correlators).

In summary, we have shown that the two emission splitting function in a physical gauge contains not only information on the triple collinear, but also the double soft and soft-collinear limits. The only obvious difference between the genuine limiting expressions and the splitting functions lies in the colour correlators and combinatorial factors. These results show the possibility to construct an NNLO-subtraction scheme with multi-emission splitting kernels in terms of a generalization of the NLO-dipole method of [28]. Schematically, the procedure would be to extract genuine limiting expressions from the results above, *e.g.* a purely collinear bit of the two emission splitting function via the subtractions

$$\left. \frac{\langle \hat{P}_{q_i g_1 g_2} \rangle}{S_{i12}^2} \right|_{CC} = \frac{\langle \hat{P}_{q_i g_1 g_2} \rangle}{S_{i12}^2} - \left. \frac{\langle \hat{P}_{q_i g_1 g_2} \rangle}{S_{i12}^2} \right|_{S_1 C_{i2}} - \left. \frac{\langle \hat{P}_{q_i g_1 g_2} \rangle}{S_{i12}^2} \right|_{S_2 C_{i1}} - \left. \frac{\langle \hat{P}_{q_i g_1 g_2} \rangle}{S_{i12}^2} \right|_{SS}. \quad (\text{B.24})$$

and then constructing a joint splitting operator as a linear combination of such expressions together with appropriate mock-up colour correlators and partitioning factors. The result would be a single operator which reproduces all limits correctly with a smooth interpolation between them. The downside to this procedure is the reconstruction of colour correlators as in Eq. (B.12) via reverse-engineering which does not guarantee the correct inclusion of colour-correlations in intermediate regions or *e.g.* the large angle soft limit [19]. In contrast, the formalism outlined in the main part of this paper avoids such features by leaving the subtractions mentioned above explicit between all topologies contributing to a given limit at a given scaling power (at the cost of having gauge-dependent intermediate expressions).

C Two emission topologies

In this section, we list the relevant topologies for two-emission processes with one and two recoilers or spectators in terms of cut diagrams. This is helpful for a visual distinction of different types of contributions, yet for the actual use in a splitting kernel we think of these diagrams in the operator-type picture from the main sections of this paper. The set of topologies presented here represent a classification of all possible amplitudes squared which arise when adding two emissions to a set of hard legs. Denoting the emissions by the fixed labels j and k , we can write this generically as

$$\begin{aligned} |\mathcal{M}_{n+2}|^2 &= \sum_i \sum_{\alpha} \left(\tilde{E}_{ijk}^{(\alpha)} + (j \leftrightarrow k) \right) \\ &+ \sum_i \sum_{l \neq i} \sum_{\alpha} \left(\tilde{A}_{ijkl}^{(\alpha)} + \tilde{B}_{ijkl}^{(\alpha)} + \tilde{X}_{ijkl}^{(\alpha)} + (j \leftrightarrow k) \right) \\ &+ \sum_i \sum_{l \neq i} \sum_{m \neq l, i} \sum_{\alpha} \left(\tilde{F}_{ijklm}^{(\alpha)} + (j \leftrightarrow k) \right), \end{aligned} \quad (\text{C.1})$$

where the respective topologies are defined below and the tilde refers to these topologies potentially being partitioned.

By the term ‘triplet’, we denote emissions off of the same emitter while ‘pairs’ denotes the emission off of two separate emitters. We find five topologies for the triplet-triplet exchange case which are shown in Fig. 3 and the six triplet-pairs in Fig. 4. Moreover, we

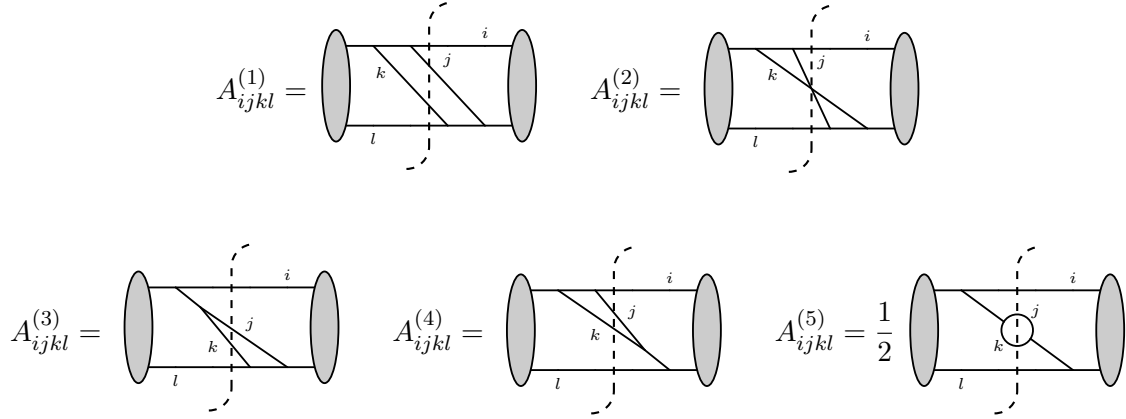


Figure 3: Triplet-triplet exchange topologies.

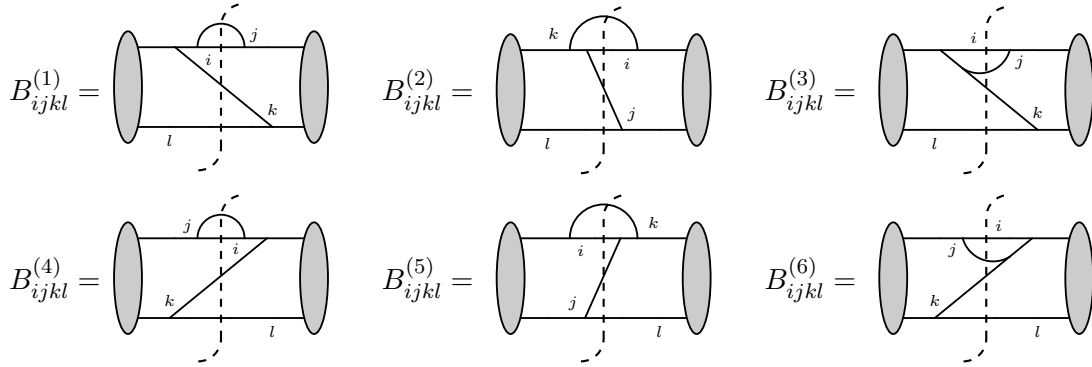


Figure 4: Triplet-pairs exchange topologies.

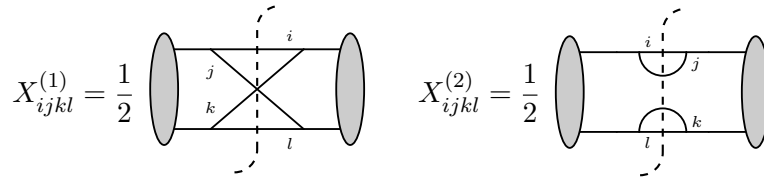


Figure 5: Pairs-Pairs exchange topologies.

have two pairs-pairs topologies as shown in Fig. 5. In addition to the exchange ones, we have self energy-type diagrams in both the triplet-triplet and pairs-pairs case, as shown in Fig. 6. Tab. 11 shows the singular propagator factors for each topology in any of the possible collinearity settings. Lastly, we have five topologies with two spectators shown in Fig. 7. Just as for the one-spectator case, we show the singular propagator factors for the two-spectator diagrams in Tab. 12.

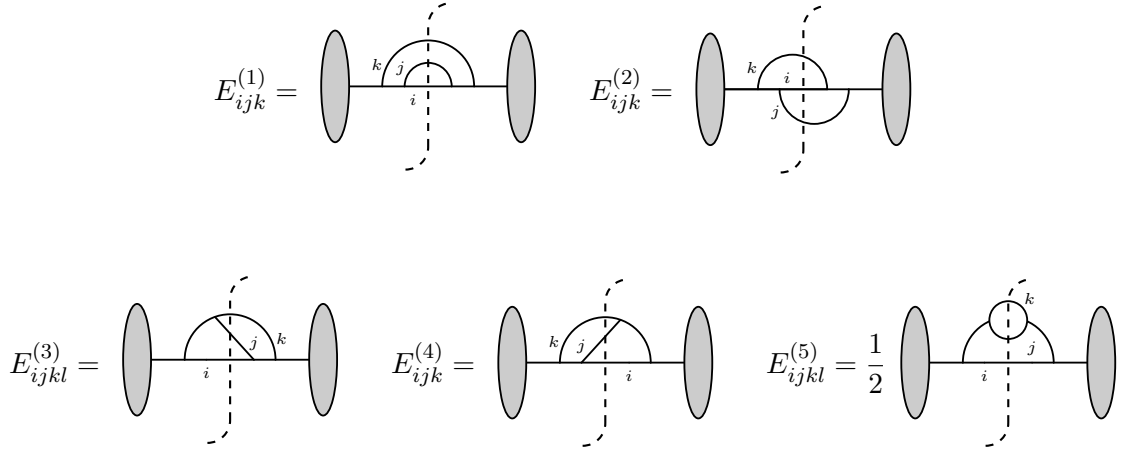


Figure 6: Self-energy like topologies.

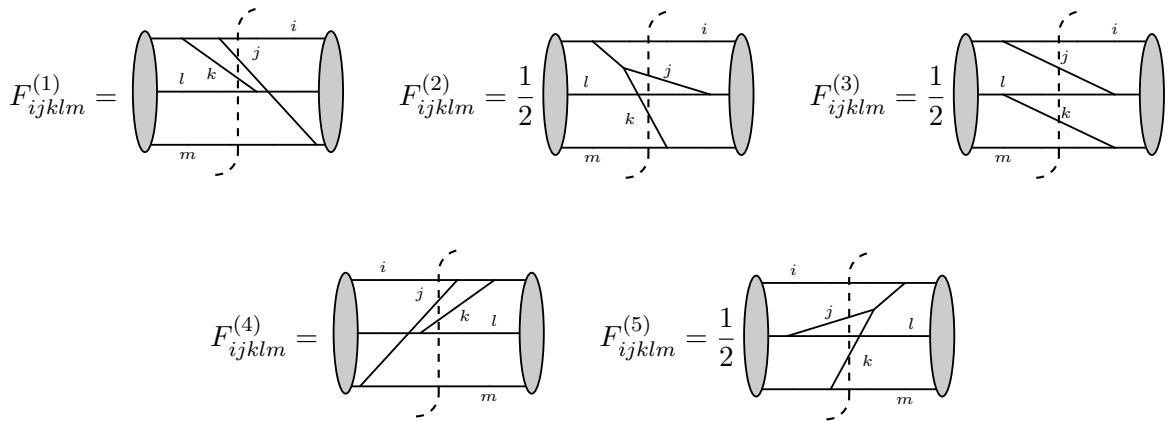


Figure 7: Two spectator topologies.

	$A_{ijkl}^{(1)}$ $S_{ij}S_{kl}S_{ijk}S_{jkl}$	$A_{ijkl}^{(2)}$ $S_{ij}S_{jl}S_{ijk}S_{jkl}$	$A_{ijkl}^{(3)}$ $S_{jk}S_{kl}S_{ijk}S_{jkl}$	$A_{ijkl}^{(4)}$ $S_{ij}S_{jk}S_{ijk}S_{jkl}$	$A_{ijkl}^{(5)}$ $S_{ijk}S_{jk}^2S_{jkl}$
$i \parallel j \parallel k$	$S_{ij}S_{ijk}$	$S_{ij}S_{ijk}$	$S_{jk}S_{ijk}$	$S_{ij}S_{jk}S_{ijk}$	$S_{jk}^2S_{ijk}$
$j \parallel k \parallel l$	$S_{kl}S_{jkl}$	$S_{jl}S_{jkl}$	$S_{jk}S_{kl}S_{jkl}$	$S_{jk}S_{jkl}$	$S_{jk}^2S_{jkl}$
$(i \parallel j), (k \parallel l)$	$S_{ij}S_{kl}$	S_{ij}	S_{kl}	S_{ij}	\times
$(i \parallel k), (j \parallel l)$	\times	S_{jl}	\times	\times	\times

	$B_{ijkl}^{(1)}$ $S_{ij}^2S_{kl}S_{ijk}$	$B_{ijkl}^{(2)}$ $S_{ij}S_{ik}S_{jl}S_{ijk}$	$B_{ijkl}^{(3)}$ $S_{ij}S_{jk}S_{kl}S_{ijk}$
$i \parallel j \parallel k$	$S_{ij}^2S_{ijk}$	$S_{ij}S_{ik}S_{ijk}$	$S_{ij}S_{jk}S_{ijk}$
$j \parallel k \parallel l$	S_{kl}	S_{jl}	$S_{jk}S_{kl}$
$(i \parallel j), (k \parallel l)$	$S_{ij}^2S_{kl}$	S_{ij}	$S_{ij}S_{kl}$
$(i \parallel k), (j \parallel l)$	\times	$S_{ik}S_{jl}$	\times

	$X_{ijkl}^{(1)}$ $S_{ij}S_{ik}S_{jl}S_{kl}$	$X_{ijkl}^{(2)}$ $S_{ij}^2S_{kl}^2$
$i \parallel j \parallel k$	$S_{ij}S_{ik}$	S_{ij}^2
$j \parallel k \parallel l$	$S_{jl}S_{kl}$	S_{kl}^2
$(i \parallel j), (k \parallel l)$	$S_{ij}S_{kl}$	$S_{ij}^2S_{kl}^2$
$(i \parallel k), (j \parallel l)$	$S_{ik}S_{jl}$	\times

	$E_{ijk}^{(1)}$ $S_{ij}^2S_{ijk}^2$	$E_{ijk}^{(2)}$ $S_{ij}S_{ik}S_{ijk}^2$	$E_{ijk}^{(3)}$ $S_{ij}S_{jk}S_{ijk}^2$	$E_{ijkl}^{(4)}$ $S_{ij}S_{jk}S_{ijk}^2$	$E_{ijkl}^{(5)}$ $S_{jk}^2S_{ijk}^2$
$i \parallel j \parallel k$	$S_{ij}^2S_{ijk}^2$	$S_{ij}S_{ik}S_{ijk}^2$	$S_{ij}S_{jk}S_{ijk}^2$	$S_{ij}S_{jk}S_{ijk}^2$	$S_{jk}^2S_{ijk}^2$
$j \parallel k \parallel l$	\times	\times	S_{jk}	S_{jk}	S_{jk}^2
$(i \parallel j), (k \parallel l)$	S_{ij}^2	S_{ij}	S_{ij}	S_{ij}	\times
$(i \parallel k), (j \parallel l)$	\times	S_{ik}	\times	\times	\times

Table 11: Collection of propagator factors giving rise to singularities w.r.t. the set of collinearity structures for two emissions with one spectator. Note that $B^{(4)}$, $B^{(5)}$ and $B^{(6)}$ have the same propagators and therefore singular factors as $B^{(1)}$, $B^{(2)}$ and $B^{(3)}$, respectively

	$F_{ijklm}^{(1)}$	$F_{ijklm}^{(2)}$	$F_{ijklm}^{(3)}$
	$S_{ij}S_{kl}S_{jm}S_{ijk}$	$S_{jk}S_{jl}S_{km}S_{ijk}$	$S_{ij}S_{kl}S_{jl}S_{km}$
$i \parallel j \parallel k$	$S_{ij}S_{ijk}$	$S_{jk}S_{ijk}$	S_{ij}
$j \parallel k \parallel l$	S_{kl}	$S_{jk}S_{jl}$	$S_{kl}S_{jl}$
$j \parallel k \parallel m$	S_{jm}	$S_{jk}S_{km}$	S_{km}
$(i \parallel j), (k \parallel l)$	$S_{ij}S_{kl}$	\times	$S_{ij}S_{kl}$
$(i \parallel j), (k \parallel m)$	S_{ij}	S_{km}	$S_{ij}S_{km}$
$(i \parallel k), (j \parallel l)$	\times	S_{jl}	S_{jl}
$(i \parallel k), (j \parallel m)$	S_{jm}	\times	\times
$(j \parallel l), (k \parallel m)$	\times	$S_{jl}S_{km}$	$S_{jl}S_{km}$
$(k \parallel l), (j \parallel m)$	$S_{kl}S_{jm}$	\times	S_{kl}

Table 12: Collection of propagator factors giving rise to singularities w.r.t. the set of collinearity structures for two emissions with three hard lines i, l, m . Note that $F^{(4)}$ and $F^{(5)}$ have the same singular factors as $F^{(1)}$ and $F^{(2)}$, respectively.

D Removal of non-leading singular contributions

In order to construct the object $\hat{\Delta}_{\bar{r}}^r$ in Eq. (2.17), we start with a decomposition of one as in $1 = \delta_j^i + \bar{\delta}_j^i$, using the usual Kronecker-delta and

$$\bar{\delta}_j^i \equiv 1 - \delta_j^i. \quad (\text{D.1})$$

The indices in δ_j^i and $\bar{\delta}_j^i$ refer to having external parton lines i on the amplitude side and j on the conjugate side of a diagram being connected (to either an emitter, emission or interferer line) or disconnected (meaning connected to a hard external line which does not affect any singular limit), respectively. This decomposition reads

$$\hat{D}_{\bar{r}}^r \equiv \frac{1}{n_\sigma} \sum_{\sigma} \prod_{g=1}^{\min(p, \bar{p})} \prod_{l=1}^{l_g} \left(\delta_{\sigma(\bar{r}_{gl})}^{r_{gl}} + b_{\sigma(g)} \bar{\delta}_{\sigma(\bar{r}_{gl})}^{r_{gl}} \right), \quad (\text{D.2})$$

where σ stands for permutations of the set $\bar{S}_{n,p,k}$ and n_σ is the number of permutations.⁶ In this expression, the index g numbers the splitting groups and l_g represents the length of each group. Then, Eq. (D.2) serves as a generating function where the parameters b_g are used to control the number of unconnected lines in each group of splitters (*i.e.* between singular partons of the amplitude side complex conjugate one), *viz.* in

$$\hat{\Delta}_{\bar{r}}^r \equiv \sum_{n=0}^{\min(p, \bar{p})} \sum_{\bar{g}=1}^{\bar{p}} \frac{\partial^n}{\partial b_{\bar{g}}^n} \hat{D}_{\bar{r}}^r \Big|_{b_{\bar{g}}=0}. \quad (\text{D.3})$$

Expanding out this objects can be used to generate the set of topologies corresponding to all diagrams of squared amplitudes that contribute in a singular setting with k emissions. Fully unconnected graphs can be neglected by setting $b_g^c = 0$ for $c > l_g$.

⁶Note that in this definition, we have implied that $p \leq \bar{p}$ and that none of the legs on the amplitudes side are unconnected.

References

- [1] S. Catani and L. Trentadue, *Resummation of the QCD Perturbative Series for Hard Processes*, *Nucl. Phys. B* **327** (1989) 323–352.
- [2] S. Catani, L. Trentadue, G. Turnock and B. R. Webber, *Resummation of large logarithms in e^+e^- event shape distributions*, *Nucl. Phys. B* **407** (1993) 3–42.
- [3] S. Catani, B. R. Webber and G. Marchesini, *QCD coherent branching and semi-inclusive processes at large x* , *Nucl. Phys. B* **349** (1991) 635–654.
- [4] G. Marchesini and B. R. Webber, *Monte Carlo Simulation of General Hard Processes with Coherent QCD Radiation*, *Nucl. Phys. B* **310** (1988) 461–526.
- [5] S. Gieseke, P. Stephens and B. Webber, *New formalism for QCD parton showers*, *JHEP* **12** (2003) 045, [[hep-ph/0310083](#)].
- [6] M. Bähr et al., *Herwig++ Physics and Manual*, *Eur. Phys. J.* **C58** (2008) 639–707, [[0803.0883](#)].
- [7] J. Bellm et al., *Herwig 7.2 release note*, *Eur. Phys. J. C* **80** (2020) 452, [[1912.06509](#)].
- [8] G. Bewick, S. Ferrario Ravasio, P. Richardson and M. H. Seymour, *Logarithmic accuracy of angular-ordered parton showers*, *JHEP* **04** (2020) 019, [[1904.11866](#)].
- [9] P. Richardson and S. Webster, *Spin Correlations in Parton Shower Simulations*, *Eur. Phys. J. C* **80** (2020) 83, [[1807.01955](#)].
- [10] K. Cormier, S. Plätzer, C. Reuschle, P. Richardson and S. Webster, *Parton showers and matching uncertainties in top quark pair production with Herwig 7*, *Eur. Phys. J. C* **79** (2019) 915, [[1810.06493](#)].
- [11] M. Dasgupta and G. P. Salam, *Resummation of nonglobal QCD observables*, *Phys. Lett. B* **512** (2001) 323–330, [[hep-ph/0104277](#)].
- [12] T. Becher, M. Neubert, L. Rothen and D. Y. Shao, *Factorization and Resummation for Jet Processes*, *JHEP* **11** (2016) 019, [[1605.02737](#)].
- [13] R. Ángeles Martínez, M. De Angelis, J. R. Forshaw, S. Plätzer and M. H. Seymour, *Soft gluon evolution and non-global logarithms*, *JHEP* **05** (2018) 044, [[1802.08531](#)].
- [14] T. Gleisberg, S. Höche, F. Krauss, M. Schönherr, S. Schumann, F. Siegert et al., *Event generation with SHERPA 1.1*, *JHEP* **02** (2009) 007, [[0811.4622](#)].
- [15] S. Plätzer and S. Gieseke, *Dipole Showers and Automated NLO Matching in Herwig++*, *Eur. Phys. J. C* **72** (2012) 2187, [[1109.6256](#)].
- [16] M. Dinsdale, M. Ternick and S. Weinzierl, *Parton showers from the dipole formalism*, *Phys. Rev. D* **76** (2007) 094003, [[0709.1026](#)].
- [17] W. T. Giele, L. Hartgring, D. A. Kosower, E. Laenen, A. J. Larkoski, J. J. Lopez-Villarejo et al., *The Vincia Parton Shower*, *PoS DIS2013* (2013) 165, [[1307.1060](#)].
- [18] F. Dulat, S. Höche and S. Prestel, *Leading-Color Fully Differential Two-Loop Soft Corrections to QCD Dipole Showers*, *Phys. Rev. D* **98** (2018) 074013, [[1805.03757](#)].
- [19] M. Dasgupta, F. A. Dreyer, K. Hamilton, P. F. Monni and G. P. Salam, *Logarithmic accuracy of parton showers: a fixed-order study*, *JHEP* **09** (2018) 033, [[1805.09327](#)].

- [20] M. Dasgupta, F. A. Dreyer, K. Hamilton, P. F. Monni, G. P. Salam and G. Soyez, *Parton showers beyond leading logarithmic accuracy*, *Phys. Rev. Lett.* **125** (2020) 052002, [[2002.11114](#)].
- [21] J. R. Forshaw, J. Holguin and S. Plätzer, *Building a consistent parton shower*, *JHEP* **09** (2020) 014, [[2003.06400](#)].
- [22] K. Hamilton, R. Medves, G. P. Salam, L. Scyboz and G. Soyez, *Colour and logarithmic accuracy in final-state parton showers*, [2011.10054](#).
- [23] J. Holguin, J. R. Forshaw and S. Plätzer, *Improvements on dipole shower colour*, *Eur. Phys. J. C* **81** (2021) 364, [[2011.15087](#)].
- [24] J. R. Forshaw, J. Holguin and S. Plätzer, *Parton branching at amplitude level*, *JHEP* **08** (2019) 145, [[1905.08686](#)].
- [25] Z. Nagy and D. E. Soper, *Summations of large logarithms by parton showers*, *Phys. Rev. D* **104** (2021) 054049, [[2011.04773](#)].
- [26] S. Plätzer and I. Ruffa, *Towards Colour Flow Evolution at Two Loops*, *JHEP* **06** (2021) 007, [[2012.15215](#)].
- [27] M. De Angelis, J. R. Forshaw and S. Plätzer, *Resummation and Simulation of Soft Gluon Effects beyond Leading Color*, *Phys. Rev. Lett.* **126** (2021) 112001, [[2007.09648](#)].
- [28] S. Catani and M. H. Seymour, *A General algorithm for calculating jet cross-sections in NLO QCD*, *Nucl. Phys.* **B485** (1997) 291–419, [[hep-ph/9605323](#)].
- [29] T. Becher, A. Broggio and A. Ferroglia, *Introduction to Soft-Collinear Effective Theory*, vol. 896. Springer, 2015, [10.1007/978-3-319-14848-9](#).
- [30] A. Bassetto, M. Ciafaloni and G. Marchesini, *Jet structure and infrared sensitive quantities in perturbative qcd*, *Physics Reports* **100** (1983) 201 – 272.
- [31] L. Gellersen, S. Höche and S. Prestel, *Disentangling soft and collinear effects in QCD parton showers*, [2110.05964](#).
- [32] S. Catani, M. H. Seymour and Z. Trócsányi, *Regularization scheme independence and unitarity in qcd cross sections*, *Phys. Rev. D* **55** (Jun, 1997) 6819–6829.
- [33] I. Bierenbaum, S. Catani, P. Draggiotis and G. Rodrigo, *Feynman’s Tree Theorem and Loop-Tree Dualities*, *PoS LC2010* (2010) 034, [[1011.0585](#)].
- [34] F. Driencourt-Mangin, G. Rodrigo, G. F. R. Sborlini and W. J. TorresBobadilla, *On the interplay between the loop-tree duality and helicity amplitudes*, [1911.11125](#).
- [35] S. Plätzer, *Summing Large- N Towers in Colour Flow Evolution*, *Eur. Phys. J. C* **74** (2014) 2907, [[1312.2448](#)].
- [36] M. Löschner and S. Plätzer, “Double emission kernels for parton branching algorithms.” in preparation, 2022.
- [37] V. Del Duca, N. Deuschmann and S. Lionetti, *Momentum mappings for subtractions at higher orders in qcd*, *Journal of High Energy Physics* **2019** (Dec, 2019) .
- [38] S. Catani and M. Grazzini, *Infrared factorization of tree level QCD amplitudes at the next-to-next-to-leading order and beyond*, *Nucl. Phys.* **B570** (2000) 287–325, [[hep-ph/9908523](#)].